Flight Control Energy Saving via Helicopter Rotor Active Morphing

Tugrul Oktay*
Erciyes University, 38039 Kayseri, Turkey
and
Cornel Sultan†
Virginia Polytechnic Institute and State University, Blacksburg, Virginia 24061

DOI: 10.2514/1.C032494

Helicopter main rotor active morphing is investigated to save helicopter flight control energy in the presence of constraints on outputs. For this purpose, the nonlinear equations of motion of the helicopter are linearized around straight level flight. Then, several main rotor active morphing scenarios such as blade radius, blade chord length, blade twist angle, and rotor angular speed variation are analyzed individually (i.e., each active morphing scenario is implemented one at a time). Output-variance-constrained control is used for helicopter flight control system design, and the control energy savings due to active morphing with respect to a conventional helicopter are evaluated. An extensive circumstance in which all active morphing concepts are implemented simultaneously is examined to obtain larger control energy savings. The possibility of using morphing controls for trimming is also considered, and stochastic optimization is used to solve the resulting simultaneous trimming and control design problem. Extensive analysis, including closed-loop system responses, is carried out for the most energy-efficient active morphing procedure. Comparisons with a helicopter designed using passive instead of active morphing are also performed. Finally, some robustness properties of the closed-loop system corresponding to the active morphing scenario are examined.

Downloaded by ROKETSAN MISSLES INC. on March 21, 2014 | http://arc.aiaa.org | DOI: 10.2514/1.C032494

Nomenclature

c_b	=	blade chord length, m
J	=	control energy (cost)
p, q, r	=	helicopter angular velocities, rad/s
R	=	blade radius, m
u, v, w	=	helicopter linear velocities, m/s
$\beta_0, \beta_c, \beta_s$	=	collective and two cyclic blade-flapping angles, rad
$\zeta_0, \zeta_c, \zeta_s$	=	collective and two cyclic blade-lagging angles, rad
θ_T	=	collective tail rotor angle, rad
θ_{tw}	=	blade twist angle, rad
$\theta_0, \theta_c, \theta_s$	=	collective and two cyclic blade pitch angles, rad
ϕ_A, θ_A, ψ_A	=	helicopter Euler angles, rad
Ω	=	rotor angular speed, rad/s

I. Introduction

RECENT years have witnessed significant advances in morphing technologies due to sustained progress in a number of disciplines ranging from materials science and computation to sensing and actuation. In a continuous attempt to better mimic biological flying systems, applications of morphing concepts have lately been proposed in the design of aerospace vehicles, both at the small scale, in novel miniature air vehicles, and at the large scale, for the improvement of the performance and safety of existing flying machines. In this context, morphing techniques have recently received considerable attention from the rotorcraft community for the enhancement of several key aspects of vehicle design such as flight dynamics, vibration and noise reduction, and overall performance [1–11]. Specifically, for helicopters, remarkable progress has been made in rotor blade morphing [1–9], which consists of the ability to change some of the blade parameters. The morphing process can be classified as active or passive, according to the way actuation of morphing mechanisms is achieved. In active morphing, the morphing parameters are modified continuously during flight via feedback control, in response to sensor measurements. On the other hand, in the passive morphing scenario, there is no feedback control correlation between sensor measurements and the actuation mechanisms involved in morphing parameter modification. Therefore, active morphing enables continuous in flight adaptation to changing conditions via feedback control. Active morphing comes at the expense of more sophisticated hardware, signal processing, and control systems compared to passive morphing, but it substantially improves control capabilities and authority by expanding the number of actively controlled variables.

Various morphing concepts for helicopters, such as blade airfoil morphing, variable rotor angular speed, and variable blade radius (or length) were recently investigated. For example, in [1], it was found that, by varying the angular speed of the main rotor, the helicopter's maneuverability and agility can be improved. Also, in [3,4], this speed was allowed to vary to improve helicopter's stability. In [8], several morphing concepts (i.e., variable blade radius, blade chord length, blade twist angle, and rotor angular speed) were studied to improve total rotor power and maximum helicopter speed in cruise. A ranking of these morphing technologies for improved main rotor aeromechanics was also given in that study. It was found that, for rotor performance in cruise, the most effective morphing parameters are the variable rotor angular speed and variable blade chord length. In [11], a reliable morphing mechanism that can effectively extend the chord of a section of the helicopter rotor blade was presented. For this purpose, a morphing cellular structure was developed, and the blade chord was increased by 30%. This mechanism was first computationally designed, then also fabricated and experimentally proven to be reliable and effective.

This paper exploits and promotes these recent technological advances in the area of morphing helicopter by showing how, when combined with modern multivariable control design, they can substantially improve the overall performance, measured by the flight dynamics control energy, while also satisfying prescribed constraints. In a previous related paper [12], we showed how certain

Received 24 June 2013; revision received 13 November 2013; accepted for publication 30 November 2013; published online 24 January 2014. Copyright © 2013 by the American Institute of Aeronautics and Astronautics, Inc. All rights reserved. Copies of this paper may be made for personal or internal use, on condition that the copier pay the $10.00 per-copy fee to the Copyright Clearance Center, Inc., 222 Rosewood Drive, Danvers, MA 01923; include the code 1542-3868/14 and $10.00 in correspondence with the CCC.

*Assistant Professor, Civil Aviation School.
†Assistant Professor, Department of Aerospace and Ocean Engineering. Senior Member AIAA.

Downloaded by ROKETSAN MISSLES INC. on March 21, 2014 | http://arc.aiaa.org | DOI: 10.2514/1.C032494

main rotor morphing parameters (blade radius, blade chord length, blade twist angle, and rotor angular speed) can be used in the simultaneous design of helicopters and control systems to substantially reduce the flight dynamics control energy subject to output variance constraints. However, in [12], the morphing strategy we employed was passive. The morphing parameters were not actively controlled, being treated as additional design variables in the mixed helicopter-control system constrained optimization problem obtained when the feedback control system and helicopter were simultaneously designed. On the other hand, in this paper, main rotor active morphing is investigated. Therefore, morphing parameters augment the helicopter control vector and are embedded in the overall control strategy. One major consequence is that the number of active helicopter controls used in this paper grows from the conventional four (collective, two cyclics for the main rotor, and tail rotor control) to a maximum of eight when all main rotor morphing concepts are considered (collective, two main rotor cyclics, and tail rotor control as well as main rotor blade radius, blade chord length, blade twist angle, and rotor angular speed). These novel morphing concepts, which enable in-flight active modification of the blade radius, blade chord length, blade twist angle, and rotor angular speed for the main rotor, are studied to minimize the control energy of the helicopter flight control system while also ensuring satisfaction of variance constraints on certain outputs.

For the study presented in this paper, physics-based control-oriented helicopter models were developed. A description of our general control-oriented modeling philosophy and process is given in [13], and more details can be found in [14]. The key idea is that the model development process must capture the "essential helicopter" dynamics using equations that require minimal processing for control design. By essential dynamics, we refer to dynamics that is directly affected by control effectors, even though the control system's design goal does not specifically include dynamic effects associated with control effectors. For example, for flight control system design, usually only the flight dynamics modes and closely related states are of interest (e.g., fuselage states), but the control effectors are intimately connected to the blade dynamics. When these effectors are used for the flight control task, they clearly influence blade dynamics. Therefore, even though blade dynamics is not of direct interest to the flight control system design process, it must be captured and monitored to ensure safe operation of the helicopter. Essential dynamics thus includes dominant blade dynamics, such as blade flapping and lead–lagging motions, and eventually blade flexibility [13,14]. Furthermore, to facilitate control design and minimize costly precontrol processing, the equations of motion should be directly derived as ordinary differential equations (ODEs) because such equations are amenable to control design. This was achieved via appropriate modeling assumptions combined with a lumped system modeling strategy (see [13,14] for details).

Several helicopter flight control system design techniques were investigated throughout the years, such as (in historical sequence) classical pole placement methods [15–17], simple feedback control approaches [18–20], modern control methods based on linear matrix algebra like the linear quadratic regulator and linear quadratic Gaussian (LQG) approaches [21–24], or H_∞ control synthesis [25–27]. In this paper, a modern control strategy, namely output-variance-constrained control is applied to design the helicopter control system. Output-variance-constrained controllers are LQG-type controllers with a special selection of the output weighting matrix. This selection guarantees satisfaction of prescribed upper bounds on the variance of specified outputs, even for strongly coupled, large multi-input/multi-output systems, like the ones encountered in our helicopter work. We recently showed that output-variance-constrained controllers are effective in helicopter control, investigated their performance when sensors fail, and indicated that sensor failure mitigation is possible by switching between such controllers [28]. We also used output-variance-constrained controllers in our previous work that exploited passive main rotor morphing for simultaneous helicopter and control system design [12].

As already mentioned, when active morphing is used, the number of control variables increases by adding morphing controls to the control vector. This has two major consequences. First, the size of the controller increases compared to the conventional helicopter, making control design and implementation more challenging. The second consequence is related to trimming the morphing helicopter, which in this paper means finding solutions to straight level flight conditions. The number of trim unknowns increases with the addition of morphing controls; however, no additional trim equations are added. Therefore, to solve the nonlinear trim equations in this paper, two approaches are taken. In the first one, the trim morphing parameter values are fixed, leading to a determined trim system in which the number of equations is equal to the number of unknowns. Then, once the trimming problem is solved, the corresponding linearized equations of motion are used for control design. It is clear that, in this approach, only the small variations of morphing parameters from their nominal values are used in feedback control design. In the second approach, the trim morphing parameters are not fixed, and so the trim system is underdetermined (i.e., it has more unknowns than equations), and it can be solved for the trim values of states and conventional control parameters as functions of the trim morphing parameters. Therefore, the trim morphing parameters become additional optimization variables that are used in the control design phase. Thus, in this approach, both the trim values of the morphing parameters and their small variations from these trim values are used in control design. Clearly, this second approach is more computationally demanding. For its solution, a stochastic optimization technique, namely the simultaneous perturbation stochastic approximation (SPSA) [29,30] method, is used to get the trim values that are most efficient for control energy reduction. SPSA was selected because it is computationally inexpensive and very effective in solving constrained optimization problems when it is not possible to compute derivatives (e.g., gradients, Hessians) analytically, as is the case herein. We also successfully used SPSA to determine optimum design parameters (e.g., blade radius, rotor angular speed, blade-flapping spring stiffness, etc.) for simultaneous design of helicopter and control system in [12].

In this paper, first the following main rotor active morphing scenarios are analyzed individually: blade radius, blade chord length, blade twist angle, and rotor angular speed variation. This means that each of these active morphing scenarios is implemented one at a time. The helicopter is trimmed assuming that the trim morphing parameters are fixed to their nominal values, control design is performed using linearized models, and the control energy savings with respect to the conventional helicopter, which does not use morphing, are computed. This study allows ranking of the individual active morphing parameters. Next, all active morphing parameters are simultaneously implemented, the trimming problem is similarly simplified by assuming fixed values of the trim morphing parameters, the control design process repeated, and the energy saving computed. Finally, the trim morphing parameters are not fixed, and they are also used for trimming the helicopter, which leads to a simultaneous trimming and control design problem, solved using SPSA as summarized in the previous paragraph. Because the resulting design is most performant in terms of control energy, our study focuses on this last scenario. An extensive analysis of closed-loop responses is presented, different flight conditions are investigated, and comparisons with a passive morphing helicopter design performed in [12] are conducted. Robustness properties of the active morphing helicopter are also investigated with respect to modeling uncertainties (i.e., flight conditions and helicopter inertial parameters variations), leading to the evaluation of controllers that are aware and unaware of the flight condition.

II. Helicopter Model

The helicopter modeling approach used to generate the models employed in this paper was presented in detail in [13,14] and is briefly summarized here. The key modeling assumptions are listed next. First, the helicopter was treated as a multibody system including all of the typical helicopter components, i.e., fuselage, empennage (tail rotor hub and shaft and horizontal tail plane), landing gear, fully articulated main rotor with four rigid blades with blade flapping and

Table 1 Comparison of flight dynamics modes (radians per second)

	Hover		40 kt		80 kt	
Mode	Our model	Padfield [32]	Our model	Padfield [32]	Our model	Padfield [32]
First	$0.2215 \pm 0.5966i$	$0.2772 \pm 0.5008i$	$-0.0434 \pm 1.0846i$	$-0.1543 \pm 0.9181i$	-0.1736 ± 2.0642	$-0.1854 \pm 1.0546i$
Second	$0.0587 \pm 0.3589i$	$-0.0410 \pm 0.5691i$	$-0.0143 \pm 0.3253i$	$0.0275 \pm 0.3185i$	$-0.0138 \pm 0.1674i$	$-0.0085 \pm 0.2074i$
Third	-0.1449	-0.2697	-0.0703	-0.0976	-0.04786	-0.1358
Fourth	-1.1944	-0.3262	-0.7140	-0.9817	-0.7587	-1.5163
Fifth	$-0.6536 \pm 0.3536i$	$-1.2990 \pm 0.2020i$	$-0.6125 \pm 1.1300i$	$-1.0394 \pm 0.2798i$	$-0.6759 \pm 1.8865i$	$-0.9252 \pm 1.0503i$

lagging hinges, and a tail rotor [13,14]. A Pitt–Peters static inflow formulation was used for the main rotor inflow (see [31]), and linear incompressible aerodynamics was assumed for the blades, whereas for the fuselage an analytical aerodynamics formulation was used. The modeling process involved application of physics principles, and because of the aforementioned modeling assumptions, it directly led to dynamic models composed of finite sets of ODEs. As discussed before, this mathematical structure is very useful for control design because it facilitates the direct use of modern control theory, which relies on state–space representations of the system's dynamics, easily obtained from ODEs.

The modeling methodology described before was implemented in Maple and led to a nonlinear helicopter model in implicit form:

$$f(\dot{x}, x, u) = 0 \tag{1}$$

where $f \in \mathbb{R}^{28}$, $x \in \mathbb{R}^{25}$, and $u \in \mathbb{R}^4$. Here, x and u are nonlinear state and control vectors, respectively, and $\mathbb{R}^*$ denotes the linear space of $*$-dimensional real vectors, where $*$ can be 4, 25, or 28. Note that the discrepancy between the size of $f(28)$ and the size of $x(25)$ is due to the three static downwash equations. The 28 nonlinear equations in Eq. (1) are classified as follows: nine fuselage equations, 16 blade flapping and lead–lagging equations, and three static main rotor downwash equations. This model has too many terms, making its use in fast computation impossible. Therefore, a systematic model-simplification method, called the ordering scheme, was applied to reduce the number of terms in the nonlinear ODEs. The ordering scheme iteratively eliminates terms from an equation based on their relative magnitude with respect to the other terms in that equation. Each term's magnitude is estimated based on expected values that the state and control variables can have during helicopter flight; see [13,14]. It is important to note that the ordering scheme does not alter the type or number of equations generated using physics principles; it only shortens the equations by retaining the dominant terms.

The model obtained after application of the ordering scheme is still fairly complex, with a total of 28 nonlinear equations. For control design, in this paper, we considered that the nominal trajectories are straight level flights. When the straight level flight conditions were introduced in the nonlinear equations of motion, 17 trim equations were obtained (i.e., $0 = 0$ equations were eliminated). These trim equations were solved using Matlab for different straight level flight conditions. After trimming, the model was linearized using Maple, yielding continuous linear time-invariant (LTI) systems:

$$\dot{x}_p = A_p x_p + B_p u_p \tag{2}$$

where x_p and u_p are the perturbed states and controls. Matrices A_p and B_p are of size 25×25 and $25 \times n_u$, respectively. The state vector is composed of nine fuselage states, eight blade-flapping states, and eight blade lead–lagging states. The control vector contains three main rotor controls, collective (θ_0), longitudinal cyclic (θ_c), and lateral cyclic (θ_s) blade pitch angles, and one tail rotor (collective) control input (θ_T) as well as the additional morphing controls. As discussed in the following sections, when all morphing concepts are implemented, $n_u = 8$, whereas when only one morphing control is used, $n_u = 5$.

The Puma SA 330 helicopter (see [32]) was used to validate the models used in this paper, leading to satisfactory agreement between trim values, flight dynamics modes, and qualitatively similar flapping and lead–lagging behavior [13,14]. For completeness of this paper, we give in Table 1 some validation results that show how our model captures the dynamics of the Puma SA 330; see [14] for more validation data. For example, most flight dynamics modes (linearized system eigenvalues) of our model for hover and straight level flights with flight speeds equal to 40 and 80 kt match relatively well results reported in [32]. The mode that displays the largest differences is the fourth mode (due to modeling discrepancy between our model and [32]); however, the qualitative behavior is similar (exponentially stable mode).

The qualitative behavior of the flapping and lead–lagging modes also resembles the behavior described in [32]; the flapping modes are much farther away from the imaginary axis compared to the lagging modes, and the magnitude of the frequency bound for the flapping modes is larger than the one for the lagging modes (see Fig. 1).

We also note that all trim results showed good correspondence with data in the literature (see [13] for more details). For example, the trim values for straight level flight at a flight speed of 40 kt were

$$40\text{ kt}x_0 = [\underbrace{0.2753, 0.0370, -0.0908, 0.4857}_{\theta_{0_0}, \theta_{c_0}, \theta_{s_0}, \theta_{T_0}}, \underbrace{-0.0456, 0.0272}_{\phi_{A_0}, \theta_{A_0}}, \underbrace{0.0795, 0.0592, 0.0252, 0}_{\beta_{0_0}, \beta_{c_0}, \beta_{s_0}, \beta_{d_0}}, \underbrace{0.0218, 0.0010, -0.0082, 0}_{\zeta_{0_0}, \zeta_{c_0}, \zeta_{s_0}, \zeta_{d_0}}, \underbrace{1.2523, 6.2236, 9.2217}_{\chi_0, \lambda_{0_0}, \lambda_{c_0}}]^T \tag{3}$$

where $\{\theta_{0_0}, \theta_{c_0}, \theta_{s_0}, \theta_{T_0}\}$, $\{\beta_{0_0}, \beta_{c_0}, \beta_{s_0}, \beta_{d_0}\}$, $\{\zeta_{0_0}, \zeta_{c_0}, \zeta_{s_0}, \zeta_{d_0}\}$, and $\{\phi_{A_0}, \theta_{A_0}\}$ are trim values of conventional helicopter controls, flapping angles, lagging angles, and Euler angles, respectively, and they are all given in radians. The trim vector of linear downwash is $\{\chi_0, \lambda_{0_0}, \lambda_{c_0}\}$, where λ_{0_0}, λ_{c_0} are trims of collective and longitudinal cyclic downwash in meters per second, and χ_0 is the trim of wake skew angle given in radians.

III. Trimming the Morphing Helicopter

As mentioned before, trimming in the presence of additional controls represented by the morphing parameters leads to an underdetermined system. The simplest approach to the trimming problem is to fix the trim morphing parameters to their nominal values and solve the determined system thus obtained for the unknowns. This solution, discussed next, is equivalent to trimming a conventional helicopter, which has no morphing capabilities.

Downloaded by ROKETSAN MISSLES INC. on March 21, 2014 | http://arc.aiaa.org | DOI: 10.2514/1.C032494

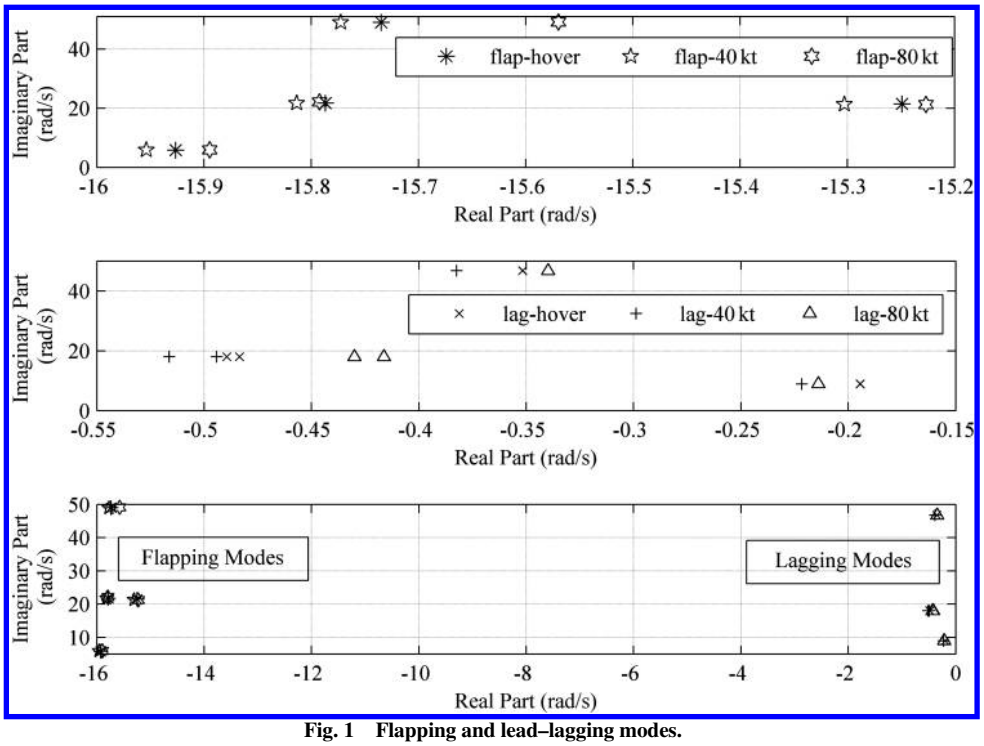

Fig. 1 Flapping and lead–lagging modes.

Four main rotor active morphing concepts are examined in this paper, simultaneously as well as separately: variable blade radius, variable blade chord length, variable blade twist angle, and variable rotor angular speed. In the simultaneous scenario, all of these morphing concepts are applied together, and so they are all included in the control vector, which has size 8. In the separate scenario, these morphing concepts are applied individually, one at a time, and so the control vector's dimension is 5.

For the "separate" scenario, the following procedure is applied to trim the helicopter. First, for the individual morphing scenario that is analyzed, the nominal value of the corresponding individual morphing element is used to trim the nonlinear system, which describes the dynamics of the helicopter with morphing main rotor. For example, if the blade chord length morphing parameter is considered, then the trim value of this morphing control is chosen 0.5401 m, which is the actual (i.e., nominal) value when morphing is not considered. The trim unknowns for this problem are roll and pitch angles of the helicopter, four blade-flapping angles (i.e., collective, two cyclic and differential angles), four blade-lagging angles (i.e., collective, two cyclic and differential angles), three main rotor conventional controls (i.e., collective and two cyclic blade pitch angles), tail rotor control (i.e., collective angle), and three main rotor downwash parameters (i.e., wake skew angle, and uniform and longitudinal cyclic components of downwash). Therefore, there are 17 trim equations for these 17 trim unknowns; see [13,14] for more details. Matlab's "fsolve" procedure was used to solve the corresponding nonlinear system, and Maple was used for linearization. For each individual morphing scenario, matrices A_p and B_p are of size 25×25 and 25×5, respectively. For the "simultaneous" scenario, all morphing concepts are applied together.

Table 2 Morphing parameters, constraints, and optimum points obtained using SPSA

Morphing parameters	Nominal value	Lower bound $\Delta x_i/x_i$	Upper bound $\Delta x_i/x_i$	Optimum trim value	Change $\Delta x_i/x_i$
c_b	0.5401 m	−0.05	0.05	0.5664 m	0.04873
R	7.5 m	−0.05	0.05	7.1250 m	−0.04999
θ_{tw}	−0.14 rad	−0.05	0.05	−0.1366 rad	−0.02455
Ω	27 rad/s	−0.05	0.05	25.6844 rad/s	−0.04873

The nominal values of morphing parameters given in Table 2 were chosen as the trim values when solving the trimming problem for the morphing helicopter. By doing so, we obtain the same 17 trim unknowns and 17 trim equations; however, the size of matrix B_p is 25×8.

In the scenarios described in the previous paragraph, the values of the morphing parameters are fixed to their nominal values when the helicopter is trimmed. By doing so, we facilitate a single solution to the trimming problem because there are as many unknowns as equations (even though the trim equations are nonlinear, only one solution was always obtained for realistic values of trim states and controls). If the morphing controls are also used for trimming, then the problem is underdimensioned: 17 equations with 21 unknowns when all morphing concepts are implemented. This gives the opportunity to use some of these unknowns (e.g., the trim morphing controls) for further optimization studies. Specifically, the 17 trim equations can be solved for the conventional trim states and controls (collective, two cyclics and tail rotor control) as functions of the trim morphing controls. Consequently, matrices A_p, B_p of the linearized model [Eq. (1)] are functions of the trim morphing controls. Therefore, we can simultaneously design a controller that meets certain specifications both over the active controller parameters and over the trim values of the morphing controls. In the following, this is referred to as the "simultaneous trimming and control design" problem for the morphing helicopter. The mathematical description of this new problem requires selection of a control design procedure, and so we first present the control system design procedure used in this paper, and in the following section, we completely describe the simultaneous trimming and control design problem.

IV. Control System

One of the main as well as traditional goals of control design is minimization of control energy. In addition, realistic control system design should take into account constraints (e.g., on the control inputs, outputs, or other variables). Therefore, in this paper, we employ a modern control technique, which minimizes control energy while also guaranteeing satisfaction of variance constraints on the output variables. This technique, known as output-variance-constrained control (OVC) [33–38], was also successfully used in our previous paper on passive morphing (i.e., simultaneous helicopter and control design) [12] and in our study on sensor failure

Downloaded by ROKETSAN MISSLES INC. on March 21, 2014 | http://arc.aiaa.org | DOI: 10.2514/1.C032494

Downloaded by ROKETSAN MISSLES INC. on March 21, 2014 | http://arc.aiaa.org | DOI: 10.2514/1.C032494

management in helicopters [28]. The OVC problem's description is given here for completeness of this paper.

For a given continuous LTI system,

$$\dot{x}_p = A_p x_p + B_p u_p + w_p, \qquad y = C_p x_p, \qquad z = M_p x_p + v \tag{4}$$

and a positive–definite input weighting matrix $R > 0$, find a full-order dynamic controller

$$\dot{x}_c = A_c x_c + F z, \qquad u_p = G x_c \tag{5}$$

to solve the problem

$$\min_{A_c,F,G} E_\infty {u_p}^T R u_p \tag{6}$$

subject to

$$E_\infty y_i^2 \le \sigma_i^2, \qquad i = 1, \ldots, n_y \tag{7}$$

where z represents sensor measurements; w_p and v are zero-mean uncorrelated Gaussian white noises with intensities W and V, respectively; σ_i^2 is the upper bound imposed on the ith output variance; n_y is the number of outputs; and $E_\infty \triangleq \lim_{t\to\infty} E$, with E as the expectation operator. The quantity $J = E_\infty {u_p}^T R u_p$ is referred to as the control energy (or cost) and can be computed as $J = \text{trace}(RG\Pi G^T)$, where Π is the controller state covariance matrix (i.e., $\Pi = E_\infty x_c x_c^T$). This matrix is the lower right-hand block matrix of the closed-loop state covariance matrix $\bar{\Pi}$, obtained by solving the Lyapunov equation $A_{\text{CL}}\bar{\Pi} + \bar{\Pi}A_{\text{CL}}^T + \bar{W} = 0$. Note that the control law given by Eq. (5) is assumed to be stabilizing, and matrices A_{CL} and $\bar{W}$, which correspond to the closed-loop state $x_{\text{CL}} = [\,x_p^T \quad x_c^T\,]^T$, are very easy to construct from Eqs. (4) and (5); see also [36–38] for more details.

The solution to the OVC problem is obtained from an LQG-type problem by choosing appropriately the output weighting matrix $Q \ge 0$. Specifically, Q is dictated by the constraints imposed on the output variances, i.e., σ_i^2 in Eq. (7), and it can be obtained using the iterative algorithm described in [36–38]. After the algorithm converges and Q is found, the OVC parameters are computed using

$$A_c = A_p + B_p G - F M_p, \qquad F = X M_p^T V^{-1}$$
$$G = -R^{-1} B_p^T K \tag{8}$$

where X and K are obtained by solving the following two algebraic Riccati equations:

$$0 = X A_p^T + A_p X - X M_p^T V^{-1} M_p X + W \tag{9a}$$

$$0 = K A_p + A_p^T K - K B_p R^{-1} B_p^T K + C_p^T Q C_p \tag{9b}$$

Clearly, compared to LQG, where weighting matrices are selected ad hoc, OVC has the advantage that the weighting matrix Q is selected such that output variance constraints are satisfied.

V. Simultaneous Trimming and Control Design for the Morphing Helicopter

Now we are in the position to describe the simultaneous trimming and control design problem for the active morphing helicopter, which exploits the supplementary number of trim unknowns (i.e., the four trim morphing controls) and our ability to generate linearized models in terms of these trim morphing controls.

Let $x = \{c_b, R, \theta_{\text{tw}}, \Omega\}$ be the set of trim morphing controls. The problem of obtaining optimum trim values for these morphing controls can be obtained by altering the traditional OVC design problem described previously if we take into account the dependencies $A_p(x)$, $B_p(x)$. We emphasize that here x represents the vector of morphing controls trim values. In the control problem formulation, u_p represents perturbations of all of the controls, including the morphing controls, from their trim values. The control energy in Eq. (6) as well as all of the variance constraints in Eq. (7) are now functions of the trim morphing controls and the control matrices (A_c, F, G). Therefore, the following optimization problem is formulated:

$$\min_{A_c,F,G,x} E_\infty {u_p}^T R u_p \tag{10}$$

subject to Eqs. (4), (5), and (7). In addition, the elements of x are constrained, i.e., $x_{i_{\min}} \le x_i \le x_{i_{\max}}$ (see Table 2). This new optimization problem is more complex than OVC control design and its solution is discussed next.

VI. Simultaneous Perturbation Stochastic Approximations

The simultaneous trimming and control design problem described in Sec. V is much more difficult than the traditional OVC problem because of the introduction of the trim morphing optimization variables and the associated constraints. To solve it, we selected a stochastic optimization method (i.e., SPSA), which was successfully used in similar complex constrained optimization problems [12,14,30]. SPSA is inexpensive because it uses only two evaluations of the objective to estimate the gradient [29]. It was also successfully used in solving various constrained optimization problems [12,14,30,39]. The SPSA algorithm used here is described next.

Let x denote the vector of optimization variables. For the traditional SPSA, if $x_{[k]}$ is the estimate of x at the kth iteration, then $x_{[k+1]} = x_{[k]} - a_k g_{[k]}$, where

$$g_{[k]} = \left[\frac{\Gamma_+ - \Gamma_-}{2d_k\Delta_{[k]1}} \cdots \cdots \frac{\Gamma_+ - \Gamma_-}{2d_k\Delta_{[k]p}}\right]^T \tag{11}$$

a_k and d_k are gain sequences; $g_{[k]}$ is the estimate of the objective's gradient at $x_{[k]}$; $\Delta_{[k]} \in \mathbb{R}^p$ is a vector of p mutually independent mean-zero random variables $\{\,\Delta_{[k]1} \quad \cdots\cdots \quad \Delta_{[k]p}\,\}$ satisfying certain conditions [40,41]; and Γ_+ and Γ_- are estimates of the objective evaluated at $x_{[k]} + d_k\Delta_{[k]}$ and $x_{[k]} - d_k\Delta_{[k]}$, respectively. An adaptive SPSA algorithm that takes into account the fact that the optimization variables must be between lower and upper limits has been previously developed and combined with OVC to solve the simultaneous helicopter and control system design problem [12,14]. The adaptation is via the gain sequences a_k and d_k, which should change according to

$$a_k = \min\{a/(S+k)^\lambda, 0.95 \min_i\{\min(\boldsymbol{\mu}_{l_i}), \min(\boldsymbol{\mu}_{u_i})\}\}$$
$$d_k = \min\{d/k^\Theta, 0.95 \min_i\{\min\{\boldsymbol{\eta}_{l_i}\}, \min\{\boldsymbol{\eta}_{u_i}\}\}\} \tag{12}$$

where η_l and η_u are vectors whose components are $(x_{[k]i} - x_{\min_i})/\Delta_{[k]i}$ for each positive $\Delta_{[k]i}$ and $(x_{\max_i} - x_{[k]i})/\Delta_{[k]i}$ for each negative $\Delta_{[k]i}$, respectively. Similarly, μ_l and μ_u are vectors whose components are $(x_{[k]i} - x_{\min_i})/g_{[k]i}$ for each positive $g_{[k]i}$ and $(x_{[k]i} - x_{\max_i})/g_{[k]i}$ for each negative $g_{[k]i}$, respectively, and d, a, λ, Θ, and S are other SPSA parameters. The reader interested in the details of this algorithm is referred to [12,14]. When applied to the simultaneous trimming and control design problem, the algorithm can be summarized as follows.

Step 1: Set $k = 1$ and choose initial values for the optimization parameters, $x = x_{[k]}$, and a specific flight condition (e.g., straight level flight at speed $V_A = 40$ kt).

Step 2: Compute A_p and B_p, design the corresponding OVC using Eqs. (8) and (9), and obtain the current value of the objective, Γ_k given by Eq. (6); note that $\Gamma_k = J_k$ for OVC.

Step 3: Perturb $x_{[k]}$ to $x_{[k]} + d_k\Delta_{[k]}$ and $x_{[k]} - d_k\Delta_{[k]}$ and solve the corresponding OVC problems to obtain Γ_+ and Γ_-, respectively. Then, compute the approximate gradient, $g_{[k]}$, using Eq. (11) with d_k given by Eq. (12).

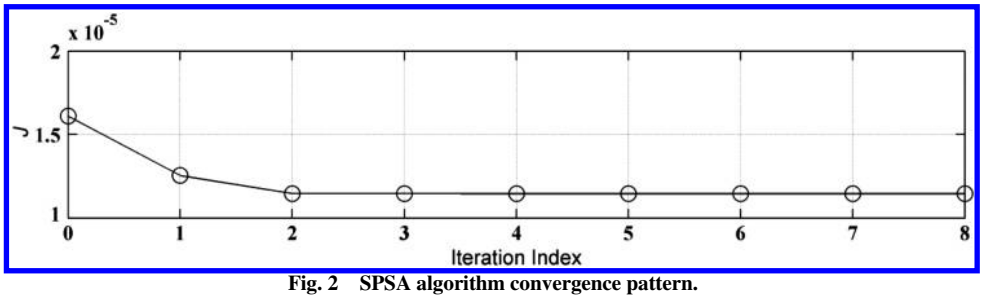

Fig. 2 SPSA algorithm convergence pattern.

Step 4: If $\|a_k g_{[k]}\| < \delta x$, where a_k is given by Eq. (12) and δx is the minimum allowed variation of x, or $k+1$ is greater than the maximum number of iterations allowed, then exit, else calculate the next estimate of x, $x_{[k+1]}$, using $x_{[k+1]} = x_{[k]} - a_k g_{[k]}$, set $k = k+1$, and return to step 2.

Because of the complicated form of the objective function, variance constraints, and nature of the algorithm, it appears that convergence cannot be guaranteed. Even for the unconstrained, traditional SPSA to guarantee convergence in probability, several conditions [29] must be satisfied, which are not easy to verify in many practical, complex problems (for example, such conditions involve three times continuous differentiability as well as uniform boundedness of the third-order derivatives of the objective function). In practice, one directly applies SPSA algorithms monitoring their performance. This was the approach we pursued in our work. As discussed in the following, the behavior of the adaptive SPSA algorithm presented before was very good, indicating that it inherits the good properties of the traditional SPSA.

VII. Results

For all of the numerical results reported next, the sensor measurements, z in Eq. (4), were helicopter linear velocities, angular velocities, and Euler angles. The outputs, y in Eq. (4), were the helicopter Euler angles. The tolerance used for all of the OVC designs was 10^{-7}.

A. Control Energy Savings

First, each of the morphing concepts was investigated individually. The nonlinear helicopter model with a morphing main rotor was trimmed and linearized around straight level flight at speed $V_A = 40$ kt for each of the individual morphing concepts as described in Sec. III. Because in this trim procedure we assume that the trim values for the morphing parameters are fixed to their nominal values, the values of the trim vector are equal to the ones when a conventional helicopter (i.e., which has no morphing capabilities) is trimmed. The trim values for all the helicopter states and conventional controls are actually given in Eq. (3), while the values for the trim morphing parameters are reported in Table 2. The A_p matrix in Eqs. (2) and (4) is the same for all scenarios investigated but the fifth column of the control matrix B_p changes according to the morphing control considered. After linearization, the corresponding OVC was designed for each of these linearized models with an output variance constraint $\sigma^2 = 10^{-4}[1 \quad 1 \quad 0.1]$ on the helicopter Euler angles, while the inputs were all of the helicopter controls (i.e., three main rotor controls and one tail rotor control) and the additional morphing control. The control energy (or cost) J_r for each of these OVCs was obtained using Eq. (6). Then, for the same flight condition, the linearized helicopter model without the morphing concept implemented was used. The OVC controller was designed for this nominal linearized model with the same output variance constraint (i.e., $\sigma^2 = 10^{-4}[1 \quad 1 \quad 0.1]$), while the inputs were only four conventional helicopter controls (i.e., three main rotor controls and one tail rotor control). The corresponding control energy was computed using Eq. (6) and labeled J_n. To evaluate the benefits of using main rotor active morphing on helicopters, the relative variation of the control energy, $\%J$, was computed using $\%J = 100(J_n - J_r)/J_n$ for each individually implemented morphing concept. The maximum energy saving was $\%J = 75.2\%$, obtained when the variable blade chord length morphing concept was considered, while the minimum energy saving (i.e., $\%J = 52.1\%$) was found when variable rotor angular speed was implemented. For the variable blade radius and twist angle morphing concepts, the relative variation of the control energy was $\%J = 61.8\%$ and $\%J = 54.7\%$, respectively.

Second, all main rotor active morphing concepts were implemented simultaneously. The nominal values of the morphing controls were used to trim the helicopter for straight level flight at $V_A = 40$ kt. Therefore, the trim values are again given by Eq. (3) and Table 2, and the state matrix A_p is the same as when each of the morphing concepts was investigated individually (see the previous paragraph). For control design, there were eight control inputs: all of the conventional helicopter controls and all of the morphing controls. The study described in the previous paragraph was repeated for OVC control design using these eight active controls, which are, of course, small perturbations from the trim values. In this case, the relative variation of the control energy was $\%J = 78.4\%$. This value is larger than all of the energy savings obtained using morphing controls separately. The only situation when the cost saving provided by a single morphing parameter implementation came closer (i.e., within 3.2%) to the cost saving provided by the application of all four morphing concepts together was for the variable chord length scenario.

Third, all main rotor active morphing concepts were used together in the simultaneous trimming and control design scenario described in Sec. V. In this case, the values of the trim morphing controls are no longer fixed but are used as additional optimization variables. The adaptive SPSA algorithm described in Sec. VI was applied to solve the simultaneous trimming and design problem using for the SPSA parameters, $S = 10$, $\lambda = 0.602$, $a = 100$, $d = 20$, and $\Theta = 0.101$. For this problem, the algorithm was very effective in rapidly decreasing the optimization cost J, converging quickly to a stable value, as seen in Fig. 2. Note that this is a particularly useful feature of SPSA, observed in other constrained optimization problems [12,29,30,39], which makes it attractive for fast solutions. Table 2 summarizes the optimization parameters, their lower and upper bounds, and optimum trim values obtained after application of the algorithm. In this scenario, the energy saving was $\%J = 84.6\%$, which is higher than in all of the previously considered scenarios (see Table 3 for comparison). These results show that the trim values of the morphing controls are highly effective on the relative variation of the control energy, and SPSA is very successful in finding optimum points fast. The vector of trim values obtained for this scenario was

$$\text{Morphing}^{40\text{ kt}}_{0} = [\underbrace{0.2976, 0.0384, -0.1143, 0.4739}_{\theta_{0_0},\theta_{c_0},\theta_{s_0},\theta_{T_0}}, \underbrace{-0.0474, 0.0406}_{\phi_{A_0},\theta_{A_0}}, \underbrace{0.0908, 0.0751, 0.0228}_{\beta_{0_0},\beta_{c_0},\beta_{s_0},\beta_{d_0}}, 0, \underbrace{0.0213, -0.0008, -0.0144}_{\zeta_{0_0},\zeta_{c_0},\zeta_{s_0},\zeta_{d_0}}, 0, \underbrace{1.2296, 7.1540, 10.3500}_{\chi_0,\lambda_{0_0},\lambda_{c_0}}]^T \tag{13}$$

Downloaded by ROKETSAN MISSLES INC. on March 21, 2014 | http://arc.aiaa.org | DOI: 10.2514/1.C032494

Table 3 Energy savings for different morphing scenarios

Individual rotor speed	Individual twist angle	Individual blade radius	Individual chord length	All morphing concepts applied together	Simultaneous trimming and control design
52.1%	54.7%	61.8%	75.2%	78.4%	84.6%

Comparison of these values with the ones in Eq. (3) shows that the trim values when morphing controls are used for trimming are very close to the ones when morphing is not used for trimming. This is important because it indicates that morphing is not dramatically changing the trim values, which remain confined to acceptable ranges.

The most important observation of this study is that the most effective main rotor active morphing scenario is when simultaneous trimming and control design is performed, leading to a maximum energy saving of $\%J = 84.6\%$. The second best scenario is when all of the morphing concepts are implemented simultaneously but morphing controls are not used for trimming ($\%J = 78.4\%$ for this situation). However, one easily remarks that both of these scenarios require extensive hardware development and the implementation of larger size controllers. Therefore, if one desires a solution with minimal hardware changes and a smaller number of controls, then the individual active morphing scenario that uses only the blade chord length is recommended ($\%J = 75.2\%$ in this case). The fact that the blade chord length variation is the most effective individual parameter in reducing the control energy is intuitively expected because the blade chord length has a significant influence on the main rotor blade aerodynamic characteristics (e.g., aerodynamic moments), which are the dominant physical mechanisms that control the helicopter motion.

B. Closed-Loop Simulations

For more in-depth evaluation of the influence of active morphing on helicopter performance, we compared the closed-loop system performance of conventional and main rotor morphing helicopters. For this evaluation, we used the main rotor morphing helicopter obtained after simultaneous trimming and control design. For the discussion to follow, we shall refer to the closed-loop system that corresponds to the conventional helicopter as the first closed-loop system (i.e., the first closed-loop system is created using the OVC designed for the conventional helicopter and coupled to the conventional helicopter). Likewise, we shall refer to the closed-loop system that corresponds to the morphing helicopter obtained using simultaneous trimming and control design as the second closed-loop system (i.e., the second closed-loop system is created using the OVC designed for the morphing helicopter and coupled to the morphing helicopter). In the next set of figures, degrees and centimeters are used to better show the behaviors of certain variables. Labels "without morphing" and "with morphing" refer to the conventional and morphing helicopter, respectively. Because linearized models are used, in all figures, variables represent perturbations from their trim values.

In Fig. 3, closed-loop responses of the outputs of direct interest for control design (i.e., helicopter Euler angles) are given when the first closed-loop system (dotted line) and second closed-loop system (solid line) are both excited by white noise perturbations. This figure shows that the closed-loop responses of helicopter Euler angles obtained using main rotor active morphing are qualitatively (i.e., shape of the response) and quantitatively (i.e., magnitude of the response) similar to the ones found without using morphing.

In Fig. 4, closed-loop responses of selected conventional controls (i.e., collective, θ_0, and two cyclic blade pitch angles θ_c and θ_s) are given for both scenarios (i.e., with and without active morphing). The most important observation regarding conventional helicopter controls (i.e., collective, two cyclics, tail rotor) is that there is significant reduction in the peaks of the absolute values of these controls if main rotor active morphing is used. Figure 4 shows that the collective pitch angle θ_0 experiences the largest reductions. Our

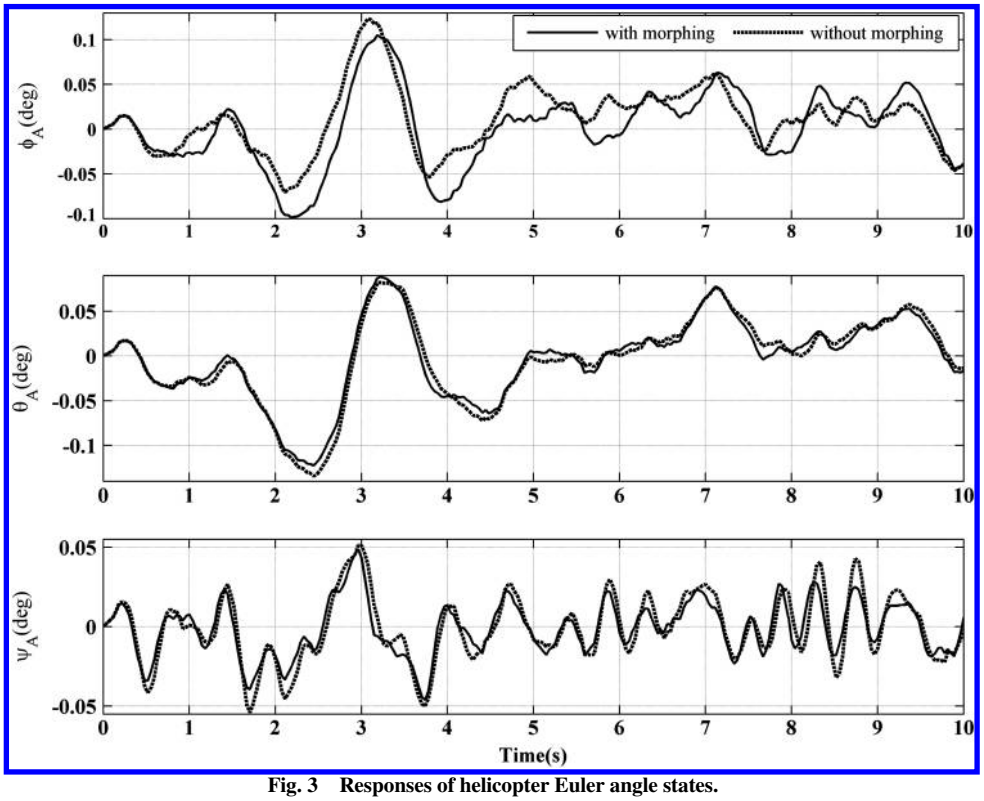

Fig. 3 Responses of helicopter Euler angle states.

Downloaded by ROKETSAN MISSLES INC. on March 21, 2014 | http://arc.aiaa.org | DOI: 10.2514/1.C032494

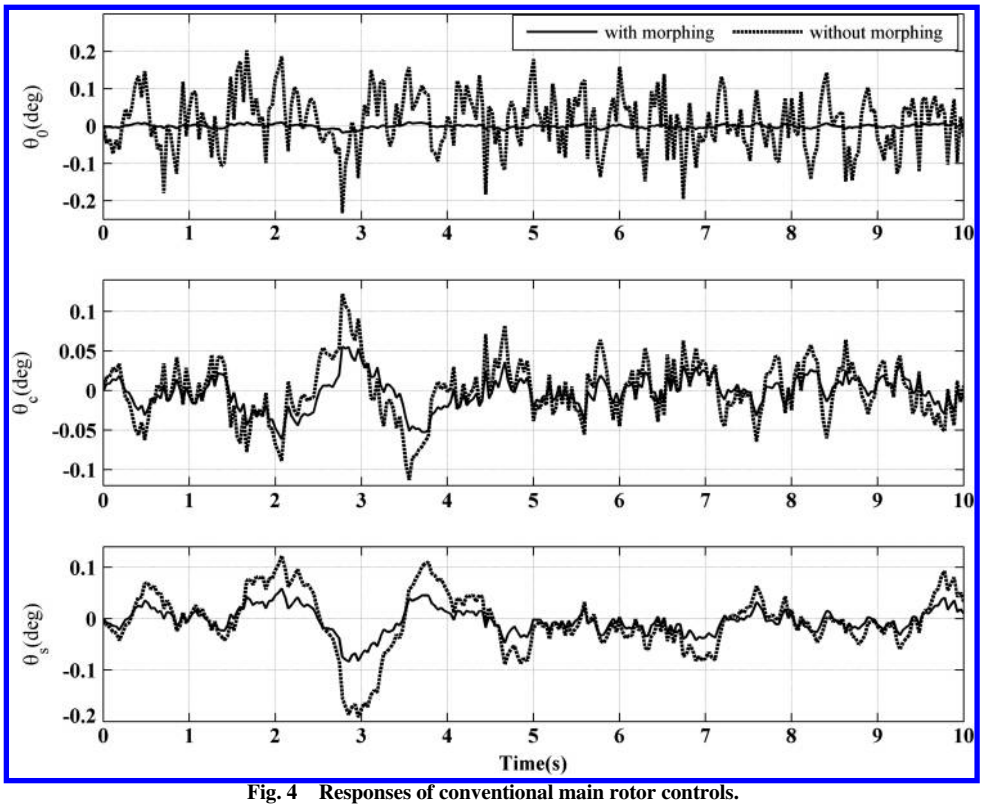

Fig. 4 Responses of conventional main rotor controls.

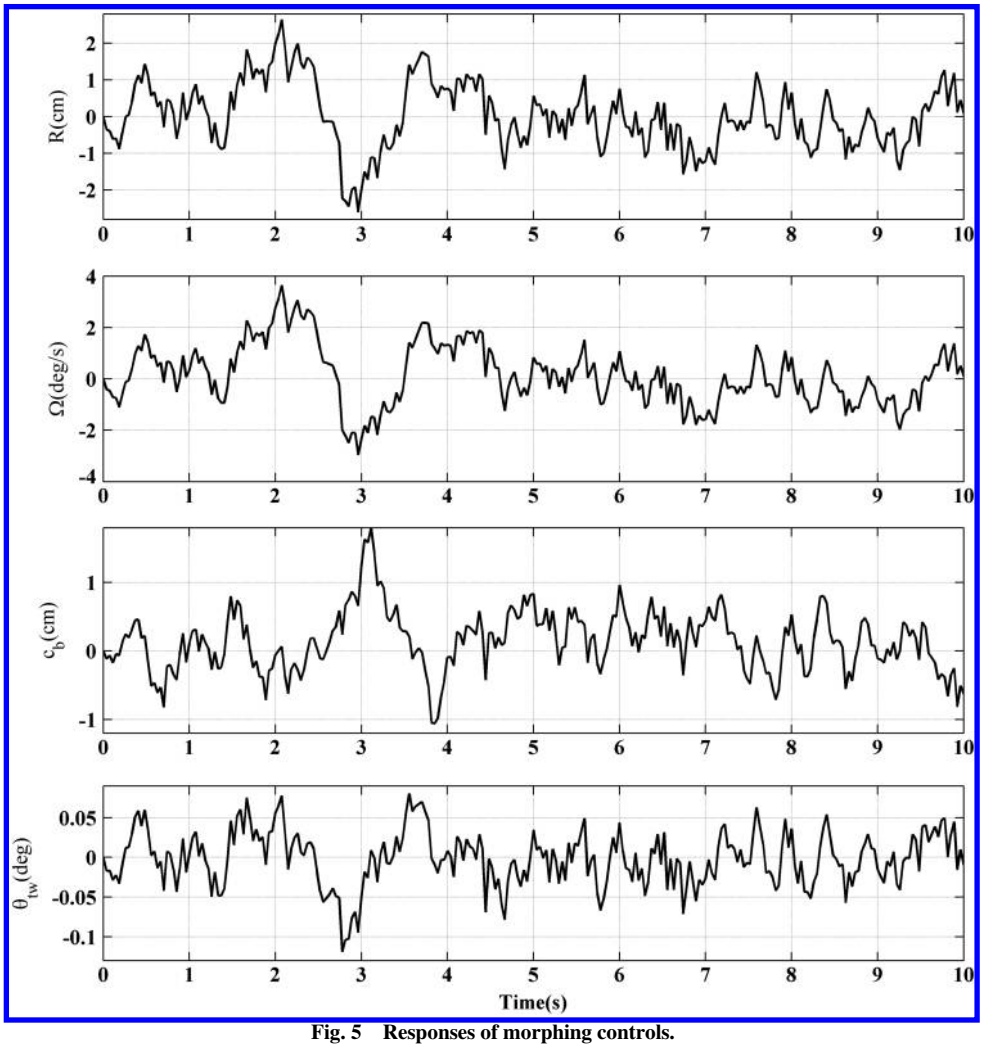

Fig. 5 Responses of morphing controls.

Downloaded by ROKETSAN MISSLES INC. on March 21, 2014 | http://arc.aiaa.org | DOI: 10.2514/1.C032494

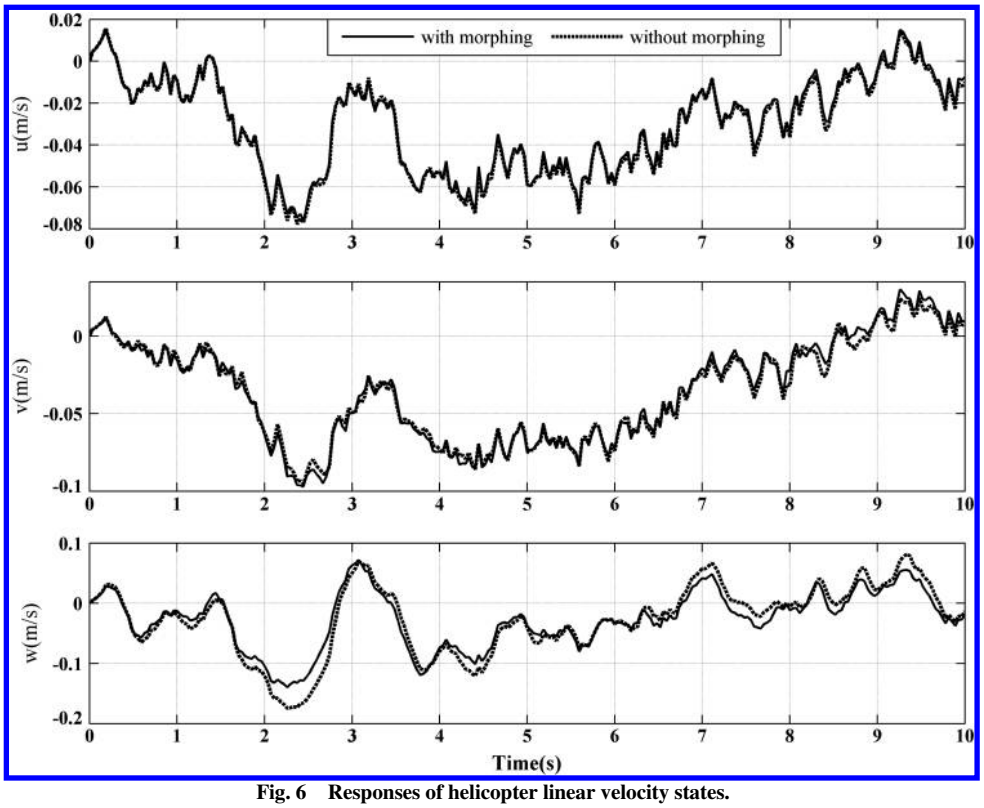

Fig. 6 Responses of helicopter linear velocity states.

extensive numerical analysis indicated that the tail rotor control experiences similar reductions. Therefore, for the main rotor active morphing helicopter, the control variations are smoother, which is always a desired characteristic. Furthermore, the significant reduction in the peaks of the absolute values of the conventional controls explains the considerable reduction in control energy observed in the previous subsection for the main rotor active morphing helicopter with respect to the conventional helicopter (i.e., $\%J = 84.6\%$).

In Fig. 5, closed-loop responses of all morphing main rotor controls (i.e., blade radius, rotor angular speed, blade chord length, and blade twist angle) are given for the second closed-loop system. It

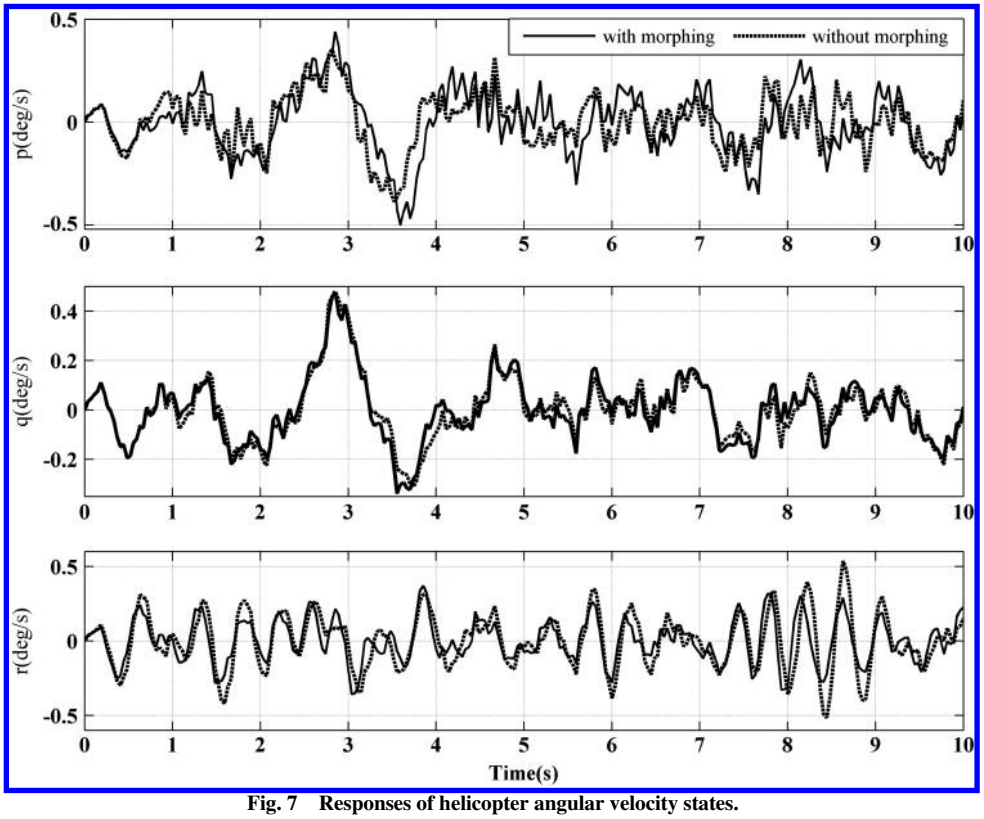

Fig. 7 Responses of helicopter angular velocity states.

Downloaded by ROKETSAN MISSLES INC. on March 21, 2014 | http://arc.aiaa.org | DOI: 10.2514/1.C032494

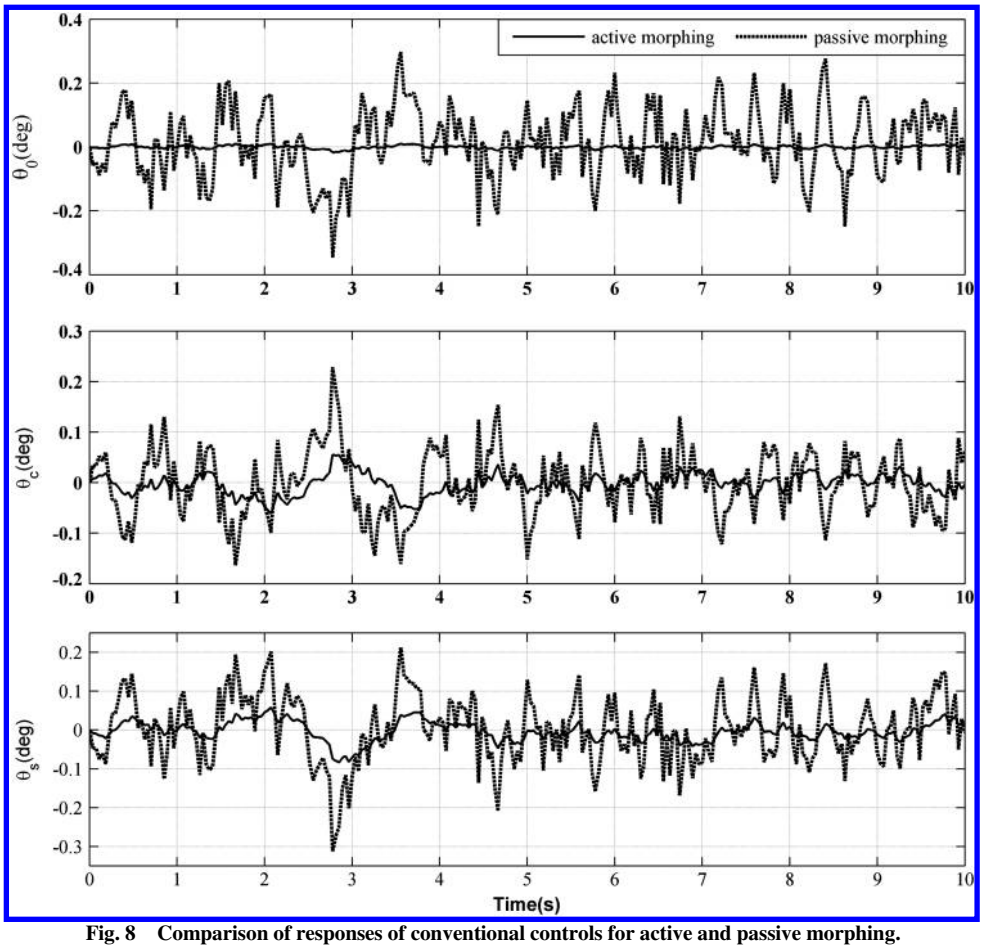

Fig. 8 Comparison of responses of conventional controls for active and passive morphing.

Downloaded by ROKETSAN MISSLES INC. on March 21, 2014 | http://arc.aiaa.org | DOI: 10.2514/1.C032494

is clear from this figure that the peaks of the absolute values of all these additional controls are very small. Therefore, the morphing controls vary within small limits around their trim values, and so they do not contribute substantially to the control energy. This observation helps to further explain the considerable energy saving obtained when active morphing is used. It should be also noted that these energy savings are slightly different from those in the real case because we used linearized models. However, the small variations from the trim values that we observe improve confidence in the accuracy of these results (i.e., for these small variations linearized models are very good approximations of nonlinear models).

In Fig. 6, closed-loop responses of some outputs that are not of direct interest for control system design (i.e., linear velocity's components on the helicopter body axes u, v, and w) are given for both scenarios (i.e., with and without morphing). None of these states experiences dangerous behavior (i.e., large and fast oscillations). Furthermore, these states qualitative and quantitative behaviors are very similar for both systems (i.e., with and without active morphing main rotor).

In Fig. 7, closed-loop responses of some other outputs that are not of direct interest for control system design (i.e., angular velocity's components on the helicopter body axes p, q, and r) are given for both scenarios. The observations we made for linear velocities are also valid for angular velocities. For example, the angular velocity states do not experience dangerous behavior, and their qualitative and quantitative behaviors are very similar.

Last, because our models have the capability to monitor the "essential dynamics" represented here by the blade states, which describe the flapping and lead–lagging motions, we also analyzed blade states responses for the closed-loop systems. Such analysis, necessary to make sure that introduction of these particular OVC controllers does not dramatically alter blade dynamics, is presented in the Appendix.

C. Comparison with Passive Morphing Design

In our previous paper [12], we studied passive morphing helicopter design. The idea was to use several free design parameters including the morphing parameters that we use in this paper (i.e., main rotor blade chord length, blade radius, blade twist angle, rotor angular speed) in a simultaneous helicopter and control system design study. The two additional design parameters used in [12] were flapping spring stiffness and blade linear mass density. Like in the current study, in [12], OVC control was also used. The problem studied here is different but a natural follow-up to the one studied in [12]; morphing controls are transformed from passive into active elements and used for simultaneous trimming and OVC control design. Therefore, some comparisons between these two studies are warranted. Most importantly, it is crucial to note that the control energy saving obtained in the passive morphing design scenario with respect to the conventional helicopter is $\%J = 33.3\%$, whereas for the best active morphing design studied in this paper, it is substantially larger: $\%J = 84.6\%$. This large difference clearly advocates for the introduction of main rotor active morphing in helicopters.

In Fig. 8, we compare responses of conventional controls (e.g., collective and two cyclics) for the helicopter endowed with active morphing designed in this paper via the simultaneous trimming and control design approach with a helicopter designed using the simultaneous helicopter and control design procedure presented in [12] (i.e., passive morphing design). The helicopter models used in the design were linearized around straight level flight at $V_A = 40$ kt. In Fig. 8, it can be easily seen that the peaks of the absolute values of all of the conventional controls for the helicopter with active morphing are much smaller than the ones for the helicopter with passive morphing design. This difference is the most important reason for the observed large difference in the energy savings mentioned in the previous paragraph.

Table 4 Morphing parameters, constraints, and optimum points using SPSA (for hover)

Morphing parameters	Nominal trim value	Lower bound $\Delta x_i/x_i$	Upper bound $\Delta x_i/x_i$	Optimum trim value	Change $\Delta x_i/x_i$
c_b	0.5401 m	−0.05	0.05	0.5670 m	0.04988
R	7.5 m	−0.05	0.05	7.1259 m	−0.04988
θ_{tw}	−0.14 rad	−0.05	0.05	−0.1470 rad	0.04988
Ω	27 rad/s	−0.05	0.05	25.6532 rad/s	−0.04988

Table 5 Morphing parameters, constraints, and optimum points using SPSA (for $V_A = 20$ kt)

Morphing parameters	Nominal trim value	Lower bound $\Delta x_i/x_i$	Upper bound $\Delta x_i/x_i$	Optimum trim value	Change $\Delta x_i/x_i$
c_b	0.5401 m	−0.05	0.05	0.5645 m	0.04512
R	7.5 m	−0.05	0.05	7.1259 m	−0.04988
θ_{tw}	−0.14 rad	−0.05	0.05	−0.1470 rad	0.04985
Ω	27 rad/s	−0.05	0.05	25.6541 rad/s	−0.04985

Table 6 Morphing parameters, constraints, and optimum points using SPSA (for $V_A = 60$ kt)

Morphing parameters	Nominal trim value	Lower bound $\Delta x_i/x_i$	Upper bound $\Delta x_i/x_i$	Optimum trim value	Change $\Delta x_i/x_i$
c_b	0.5401 m	−0.05	0.05	0.5662 m	0.04835
R	7.5 m	−0.05	0.05	7.1364 m	−0.04848
θ_{tw}	−0.14 rad	−0.05	0.05	−0.1332 rad	−0.04837
Ω	27 rad/s	−0.05	0.05	25.6908 rad/s	−0.04849

Table 7 Morphing parameters, constraints, and optimum points using SPSA (for $V_A = 80$ kt)

Morphing parameters	Nominal trim value	Lower bound $\Delta x_i/x_i$	Upper bound $\Delta x_i/x_i$	Optimum trim value	Change $\Delta x_i/x_i$
c_b	0.5401 m	−0.05	0.05	0.5256 m	−0.02676
R	7.5 m	−0.05	0.05	7.1583 m	−0.04556
θ_{tw}	−0.14 rad	−0.05	0.05	−0.1437 rad	0.02671
Ω	27 rad/s	−0.05	0.05	25.6505 rad/s	−0.04998

D. Extensive Analysis

To further improve our confidence in the advantages of main rotor active morphing as described in this paper we performed additional studies as follows. We linearized the helicopter model around hover and straight level flights at flight speeds V_A equal to 20, 60, and 80 kt. Then, we repeated the simultaneous trimming and control design for these models and computed the corresponding cost savings with respect to the conventional helicopter models. The resulting optimal values are reported in Tables 4–7, which reveal the fact that the changes from nominal values are not large (i.e., within ±5% with respect to the nominal values). Therefore, these values are tolerable from an implementation and manufacturing perspective. The energy saving ratios (i.e., $\%J$ defined in Sec. VII.A) are 76.5, 74.6, 91.6, and 94.8% for hover and 20, 60, and 80 kt for straight level flight conditions, respectively. Thus, again substantial control energy is saved if main rotor active morphing is implemented.

In Figs. 9–14, the closed-loop responses of Euler angles and controls for the linearized models of the conventional helicopter and for the helicopter endowed with main rotor active morphing are given for hover and 80 kt straight level flight conditions, respectively. We ascertain that the conclusions drawn based on the analysis for straight level flight at 40 kt are also valid in these situations. For example, the helicopter Euler angles do not experience dangerous behaviors, and the behaviors of states and controls are qualitatively similar for conventional and morphing helicopters. Moreover, there is significant reduction in the peaks of the absolute values of

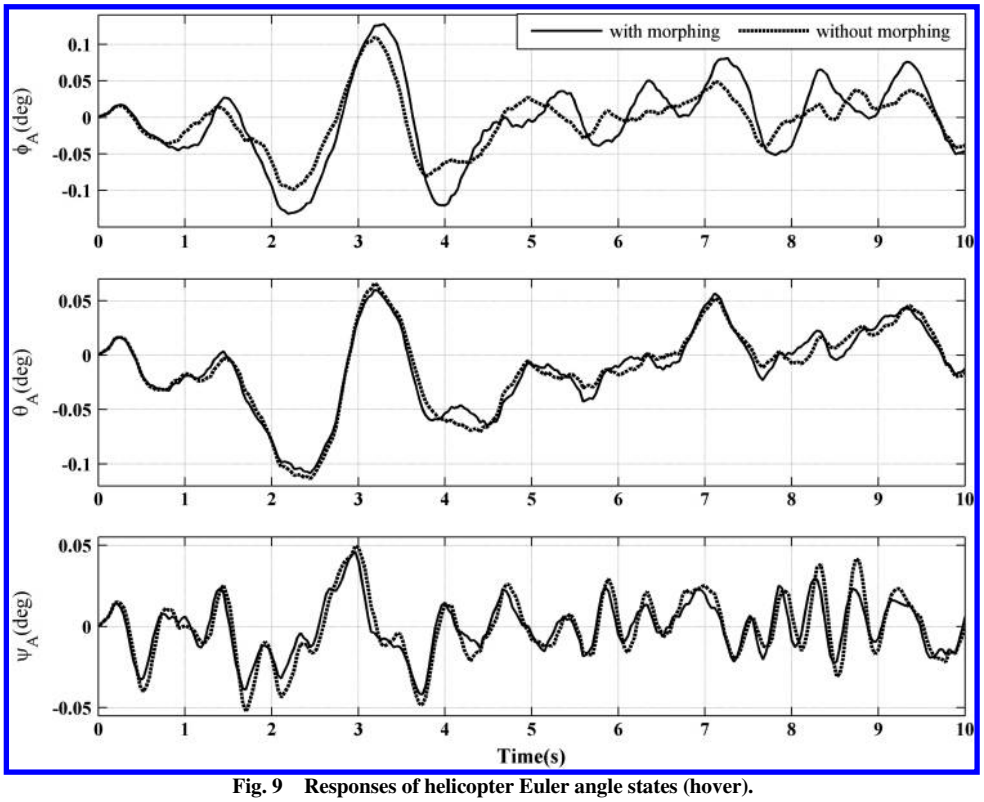

Fig. 9 Responses of helicopter Euler angle states (hover).

Downloaded by ROKETSAN MISSLES INC. on March 21, 2014 | http://arc.aiaa.org | DOI: 10.2514/1.C032494

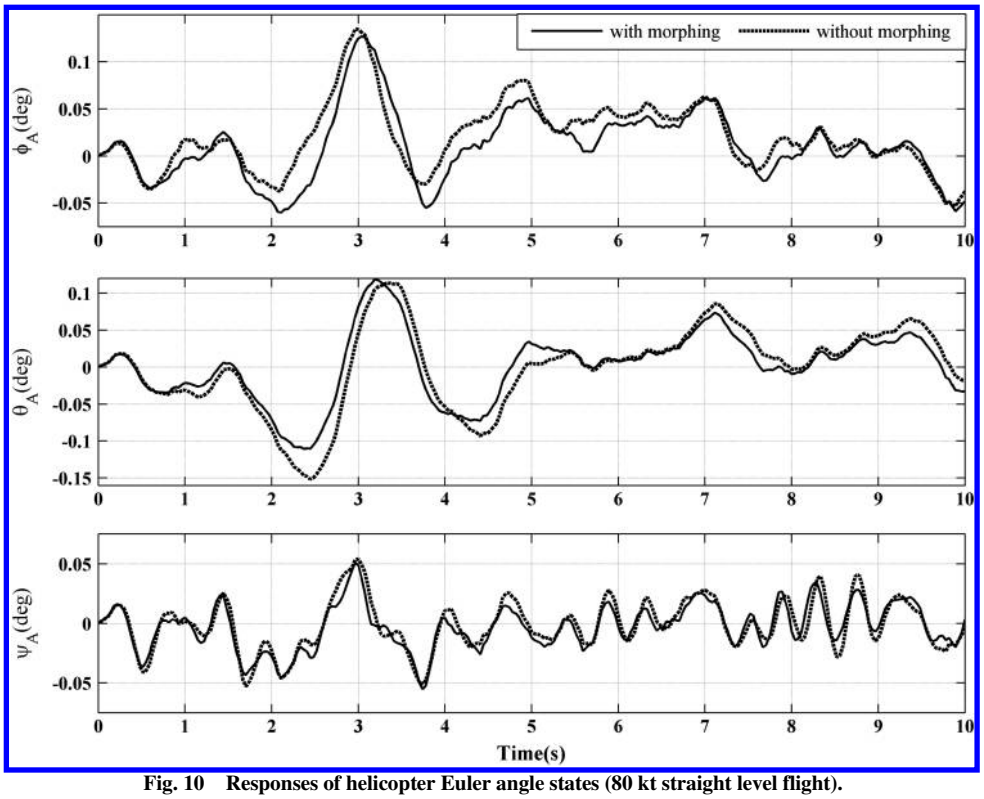

Fig. 10 Responses of helicopter Euler angle states (80 kt straight level flight).

conventional controls, while the morphing controls variations are not large, thus explaining the tremendous energy savings obtained via active morphing.

E. Robustness of the Active Morphing Helicopter System

It is well known that LQG theory does not provide guarantees on these controllers robustness (e.g., they do not have guaranteed stability margins), and so OVC controllers, as LQG controllers, inherit the same deficiency. However, the fact that the theory does not guarantee robustness does not mean that for particular designs these controllers do not have good robustness properties. Actually, in our previous works [12,28,42–45], we investigated robustness of variance-constrained controllers and found them to be quite robust when used in conjunction with our control-oriented helicopter models for applications such as sensor failure management or passive morphing. In the reminder of this paper, we focus on robustness

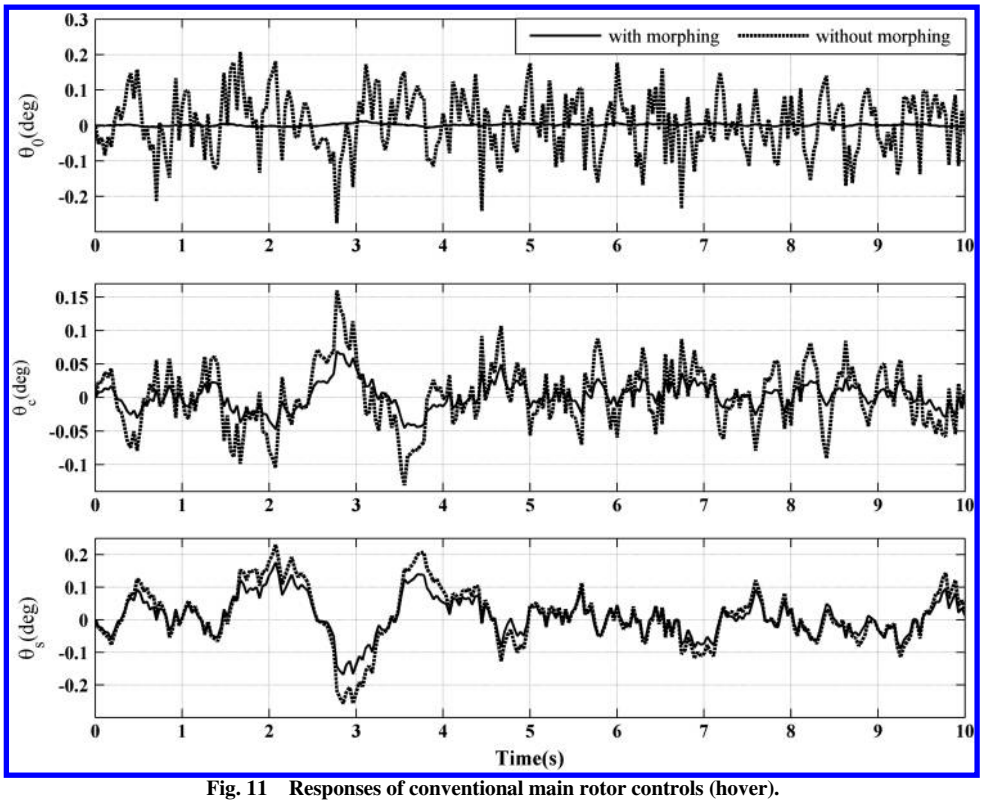

Fig. 11 Responses of conventional main rotor controls (hover).

Downloaded by ROKETSAN MISSLES INC. on March 21, 2014 | http://arc.aiaa.org | DOI: 10.2514/1.C032494

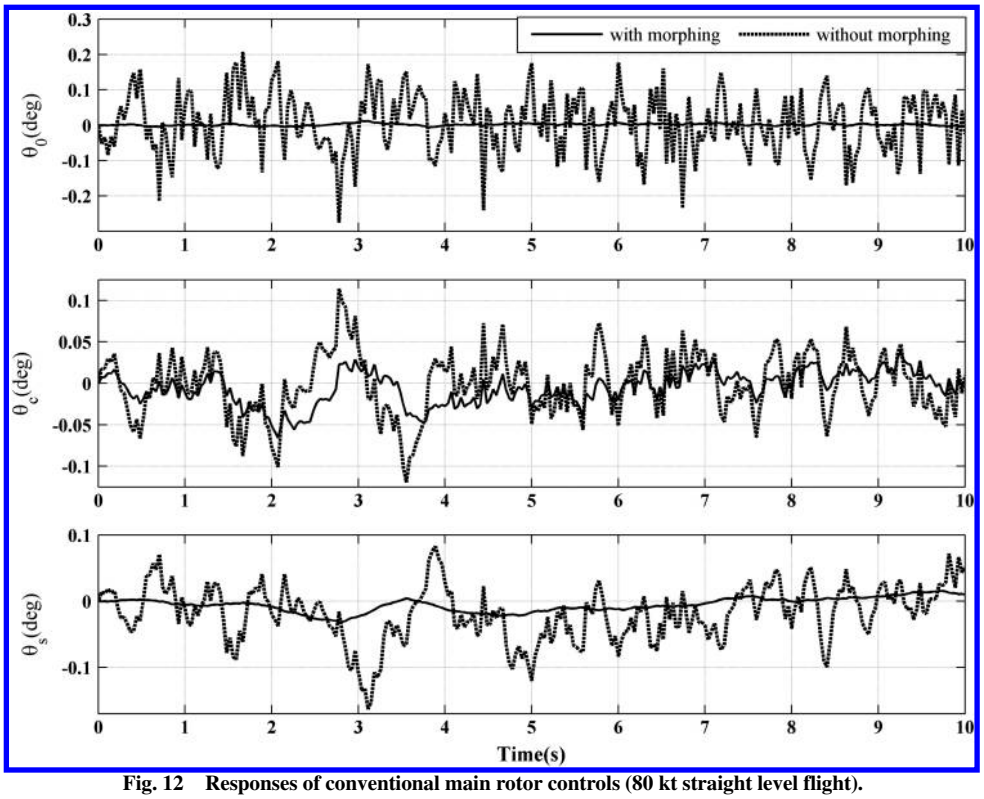

Fig. 12 Responses of conventional main rotor controls (80 kt straight level flight).

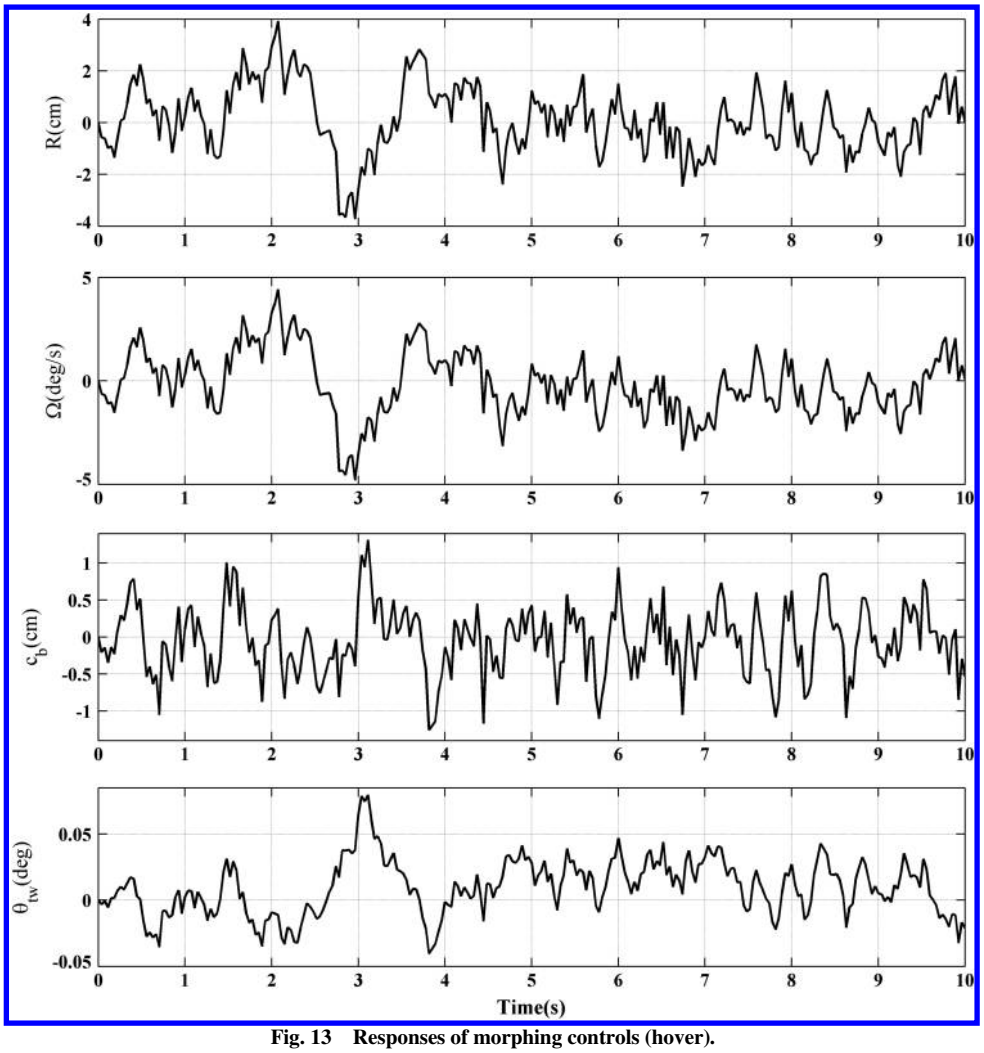

Fig. 13 Responses of morphing controls (hover).

Downloaded by ROKETSAN MISSLES INC. on March 21, 2014 | http://arc.aiaa.org | DOI: 10.2514/1.C032494

Downloaded by ROKETSAN MISSLES INC. on March 21, 2014 | http://arc.aiaa.org | DOI: 10.2514/1.C032494

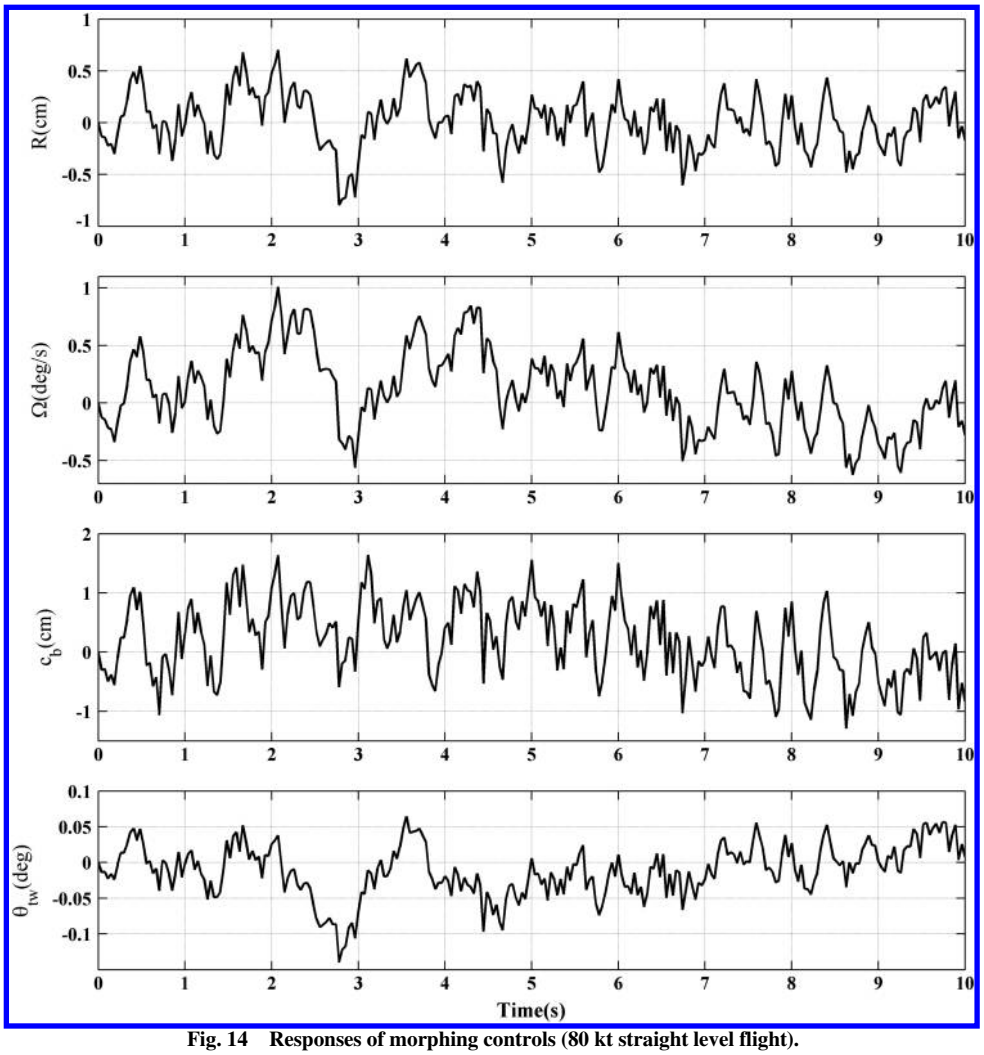

Fig. 14 Responses of morphing controls (80 kt straight level flight).

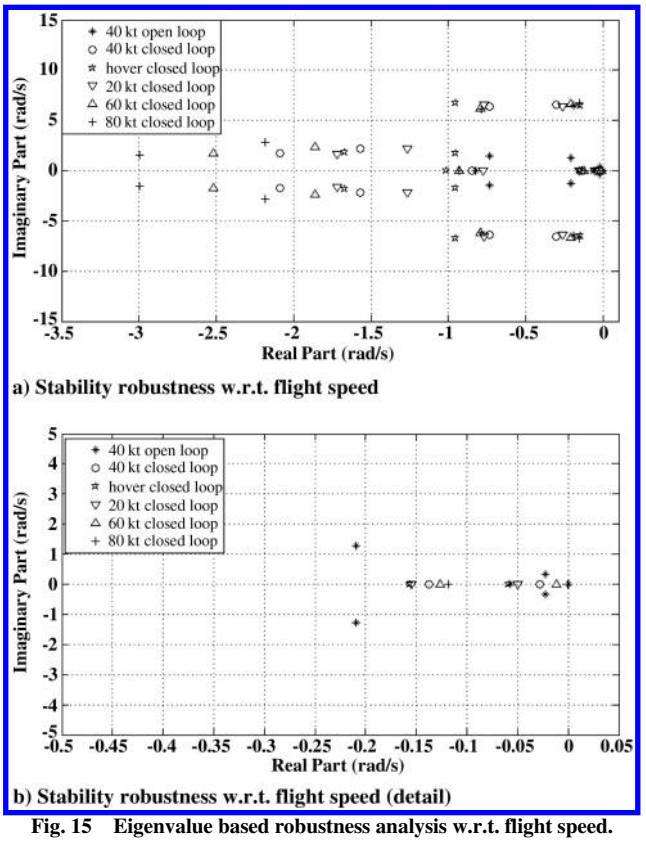

Fig. 15 Eigenvalue based robustness analysis w.r.t. flight speed.

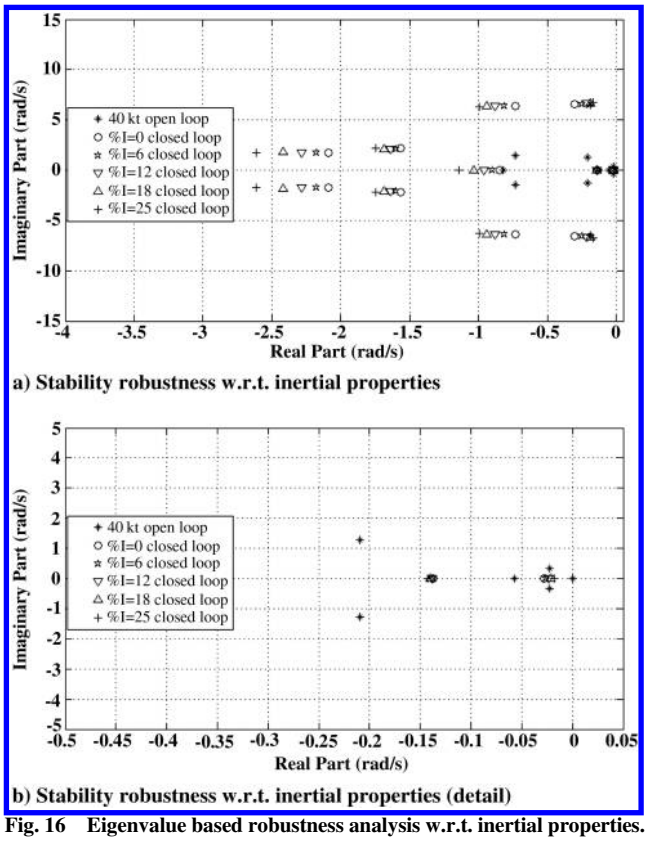

Fig. 16 Eigenvalue based robustness analysis w.r.t. inertial properties.

analysis of the helicopter endowed with active morphing main rotor implemented via OVC (i.e., the system designed in Sec. VII.A using simultaneous trimming and control design).

We analyze robustness with respect to two uncertainties: flight conditions and inertial properties of the helicopter (i.e., helicopter mass and helicopter inertia matrix). For this purpose, we first consider the following scenarios.

1) The OVC controller designed for the nominal flight condition (i.e., straight level flight at $V_A = 40$ kt) of the active morphing helicopter is used for a different flight condition (e.g., straight level flight with $V_A = 80$ kt); the inertial properties (i.e., helicopter mass and helicopter inertia matrix elements) do not change.

2) The same OVC controller like in scenario 1 is used at the same flight condition, but now all helicopter inertial parameters change.

The key question is if the corresponding closed-loop systems are still exponentially stable for these uncertainties in the flight conditions or the inertial parameters of the helicopter. This question is positively answered via a root locus analysis of the corresponding closed-loop systems, in Figs. 15, 16, where, for clarity, only the eigenvalues that are closest to the imaginary axis are represented. Figure 15a shows the location of these eigenvalues for variations up to ± 40 kt in the straight level flight speed around the nominal flight condition. In all cases, all closed-loop eigenvalues have negative real parts, indicating that the OVC controller is robustly stable with respect to (w.r.t.) such variations. Moreover, Fig. 15b shows that the most critical eigenvalues (i.e., the ones that are closest to the imaginary axis) display very small variations, indicating that they are strongly robust with respect to variations in the flight speed. Similarly, in Fig. 16, the variation of critical eigenvalues is showed when all inertial properties were varied between 0 and 25%; in this figure, $\%I$ denotes the amount by which the inertial properties were modified with respect to their nominal values. Again, strong robust stability is concluded with respect to such uncertainties.

Another interesting analysis refers to the following scenarios. First, an OVC controller is designed for the active morphing helicopter linearized around straight level flight at $V_A = 40$ kt. Then, this controller is used on the active morphing helicopter, which experiences 25% reduction in all helicopter inertial quantities, and it is linearized around a different flight condition (i.e., straight level flight at $V_A = 80$ kt). It is clear that this scenario is very challenging for the controller because it is required to operate on a system that significantly differs from the system the controller was designed for.

Downloaded by ROKETSAN MISSLES INC. on March 21, 2014 | http://arc.aiaa.org | DOI: 10.2514/1.C032494

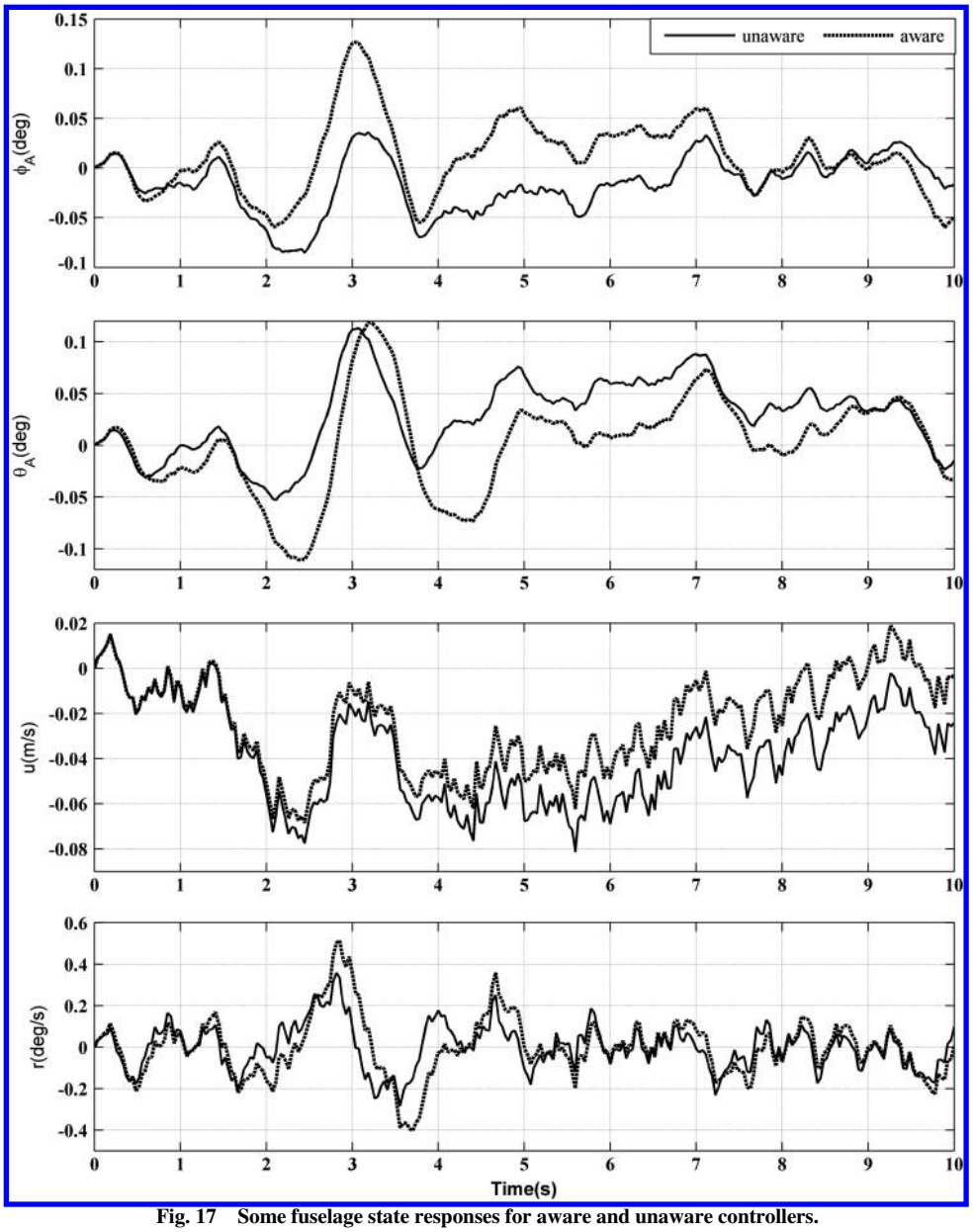

Fig. 17 Some fuselage state responses for aware and unaware controllers.

First, the new system is obtained for a different flight condition (straight level flight at $V_A = 80$ kt), and second, the corresponding helicopter model experiences rather large variations in its inertial parameters. This situation is common when there is no information (provided, for example, by a supervisory control system) about changes in flight parameters that would enable switching to a more appropriate controller. Therefore, we refer to this situation as to one in which an "unaware controller" (i.e., unaware of the flight condition) is used. On the other hand, if information is available about a substantial change in the flight condition, switching between controllers can be performed. We refer to this latter situation as one in which an "aware controller" is used. This corresponds to the scenario described next. An OVC controller is designed for the active morphing helicopter, this time linearized around straight level flight at $V_A = 80$ kt. Then this controller is used on the active morphing helicopter, which experiences 25% reduction in all inertial quantities and is linearized around the same straight level flight condition (i.e., straight level flight at $V_A = 80$ kt). This situation is encountered when a supervisory decision system exists, which ensures that, for certain flight conditions, appropriate controllers are used (i.e., aware controller).

To evaluate the performance of these aware and unaware controllers, we created the corresponding closed-loop systems. In Figs. 17–19, we give some closed-loop system-response simulations to white noise perturbations. From Fig. 17, it can be seen that, for both the aware and unaware controllers, helicopter fuselage states ranging from Euler angles (e.g., ϕ_A and θ_A) to linear (e.g., u) and angular (e.g., r) velocities have very similar behavior. We also note that their values are confined to small ranges, which is consistent with the linearization assumption made for control design (similar behaviors were ascertained for other fuselage states). Furthermore, Fig. 18 shows that helicopter blade states (e.g., β_0, β_c, ζ_0, ζ_c) have similar behavior, regardless of the fact that we use aware or unaware controllers. Also, like with the fuselage states, blade states are confined to small values and do not experience dangerous behavior. These observations reinforce our observations regarding the good robustness properties of OVC controllers for active morphing helicopters.

In terms of control responses, from Fig. 19, it can be concluded that conventional helicopter controls (i.e., θ_0, θ_c, θ_s) do not experience large variations regardless of the type of controller used (i.e., aware or unaware). Note that the same conclusions apply to the helicopter tail rotor control, while the morphing controls (not reproduced here for brevity) display very small values and variations, similarly with what was observed in Figs. 5, 13, 14. It is important to emphasize that the peaks of the absolute values of the conventional helicopter controls (especially θ_s) obtained when the unaware controller is used are

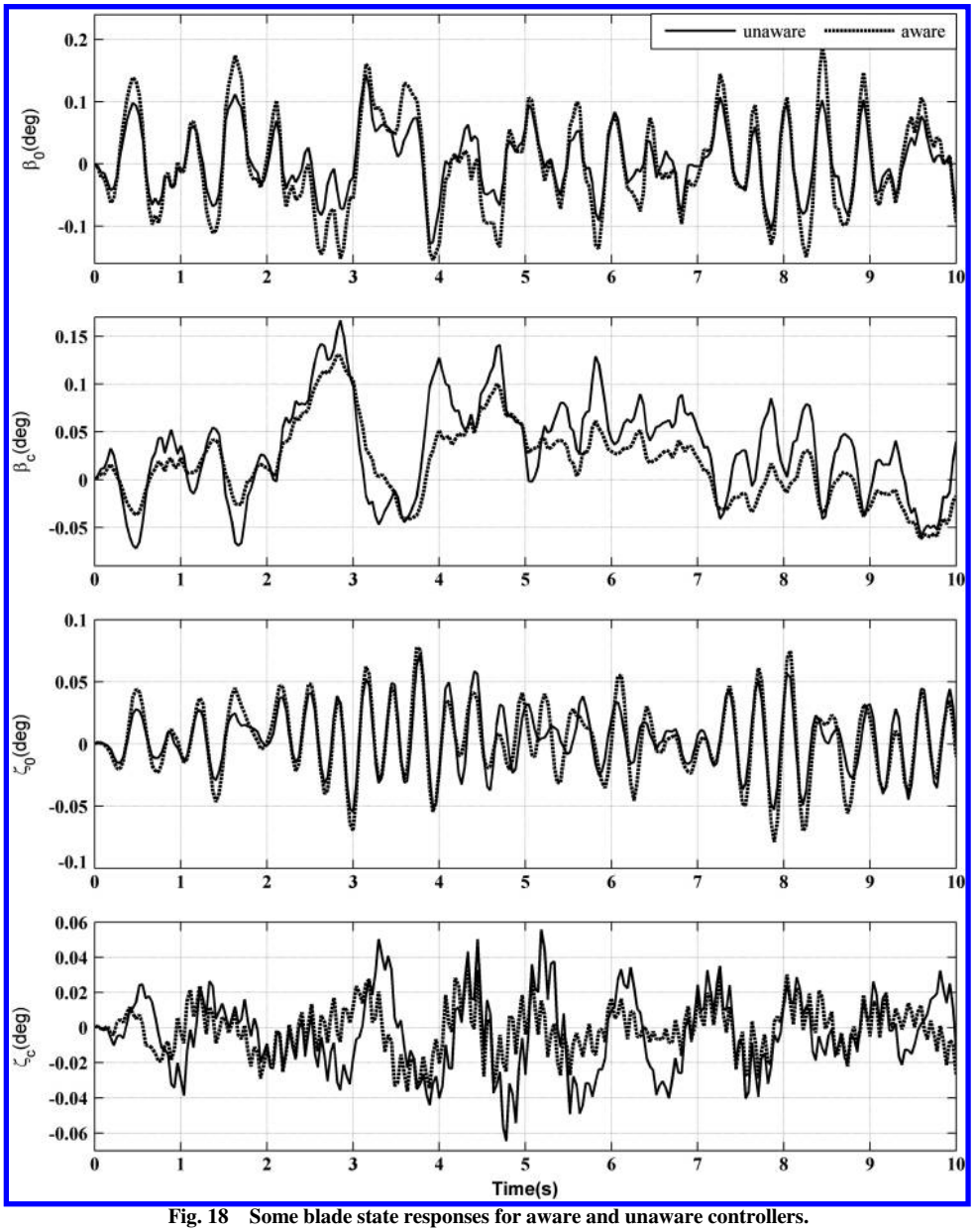

Fig. 18 Some blade state responses for aware and unaware controllers.

Downloaded by ROKETSAN MISSLES INC. on March 21, 2014 | http://arc.aiaa.org | DOI: 10.2514/1.C032494

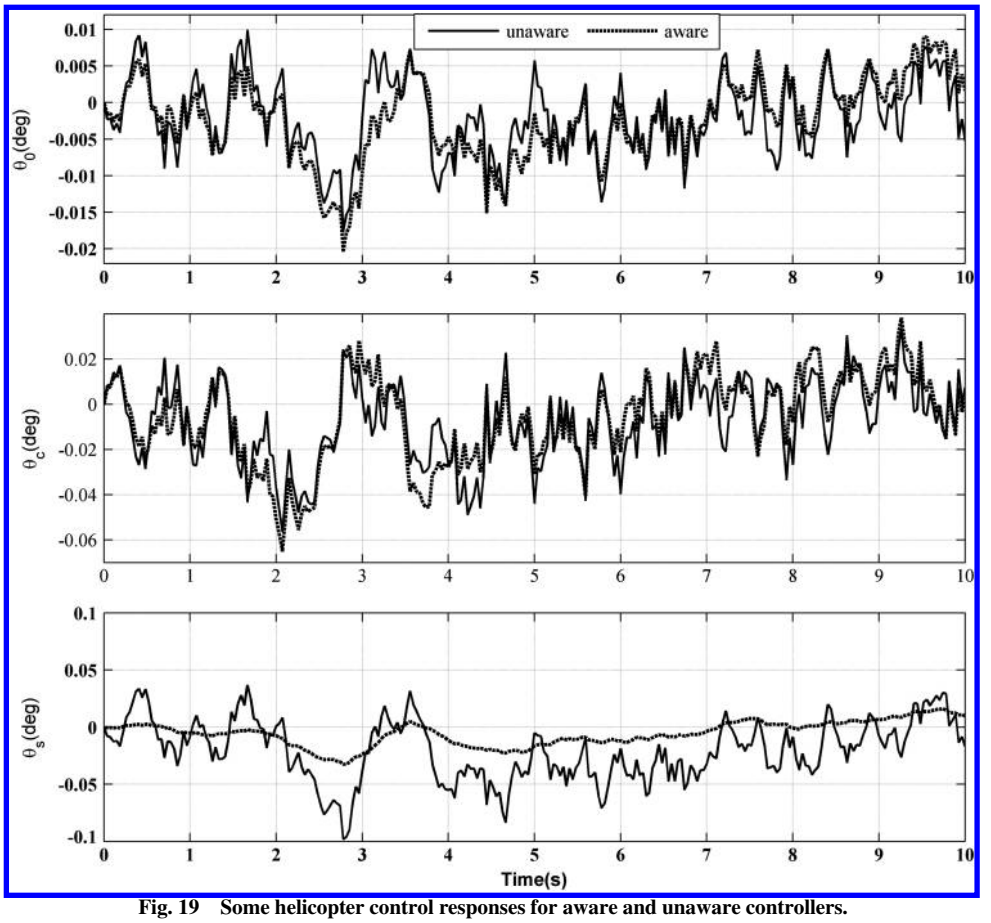

Fig. 19 Some helicopter control responses for aware and unaware controllers.

Downloaded by ROKETSAN MISSLES INC. on March 21, 2014 | http://arc.aiaa.org | DOI: 10.2514/1.C032494

generally higher than the ones obtained with the aware controller. This reveals the advantage of using aware controllers and advocates for further studies devoted to the switching mechanism (e.g., via gain scheduling) between such controllers.

VIII. Conclusions

Several main rotor active morphing concepts (i.e., blade radius, blade chord length, blade twist angle, and rotor angular speed) were thoroughly examined for flight dynamics control. For this purpose, control-oriented models developed using physics principles were used. Some validation results for a representative helicopter indicated that these models adequately capture helicopter dynamics that is relevant for flight control design.

Models linearized around straight level flight were used for the design of output-variance-constrained controllers. First, each of the active morphing concepts was applied individually (i.e., one at a time). Comparison between the corresponding control energies and the control energy of the conventional helicopter that does not use morphing led to the conclusion that variable blade chord length is the most effective morphing parameter in terms of control energy saving. Second, all morphing concepts were implemented simultaneously and two scenarios were considered. In the first scenario, for trimming, all of the morphing parameters were fixed to their nominal values, and in the second scenario, the trim values of the morphing parameters were treated as free parameters in a simultaneous trimming and control design problem. Adaptive simultaneous perturbation stochastic approximation was very effective in solving this problem. It was also concluded that the simultaneous trimming and control design scenario leads to the largest control energy reduction with respect to the conventional helicopter (i.e., 84.6%) over all active morphing scenarios considered in this paper.

For the design that resulted in the largest control energy saving, closed-loop responses revealed significantly smaller peaks of the absolute values of the conventional controls (i.e., collective, two cyclic blade pitch angles, and collective tail rotor angle) compared to the peaks corresponding to the conventional helicopter. The morphing controls variations from their trim values were also very small. These observations explain the considerable control energy reduction obtained with the active morphing helicopter. Moreover, all state (including blade state) responses did not display dangerous behavior, being confined to small variations around their trim values, as required by safe helicopter operation and by the linearization procedure used for control design. Furthermore, comparison with a helicopter design that uses passive morphing showed that the active morphing concept is superior from the control energy reduction perspective. An extensive analysis, which investigated simultaneous trimming and control design for four other flight conditions (i.e., hover and straight level flights with 20, 60, 80 kt), confirmed the superior performance of active morphing helicopters. Last, analysis of closed-loop system eigenvalues variation with flight speed and inertial properties variations revealed good stability robustness properties of the active morphing helicopter implemented via OVC. Comparison between controllers that are aware and unaware of the flight condition revealed the advantage of aware controllers, advocating for future studies in switching control.

Appendix: Blade State Responses

In Fig. A1, closed-loop responses of some blade-flapping angles (i.e., collective and two cyclic components) are given for both scenarios (i.e., with and without morphing main rotor). These states do not experience dangerous (i.e., large and fast oscillations) behavior, their variations being confined to small values around trim values. Qualitative and quantitative behaviors are similar for both helicopters (with and without morphing).

In Fig. A2, closed-loop responses of some blade lead–lagging angles (i.e., collective and two cyclic components) are given for both

Downloaded by ROKETSAN MISSLES INC. on March 21, 2014 | http://arc.aiaa.org | DOI: 10.2514/1.C032494

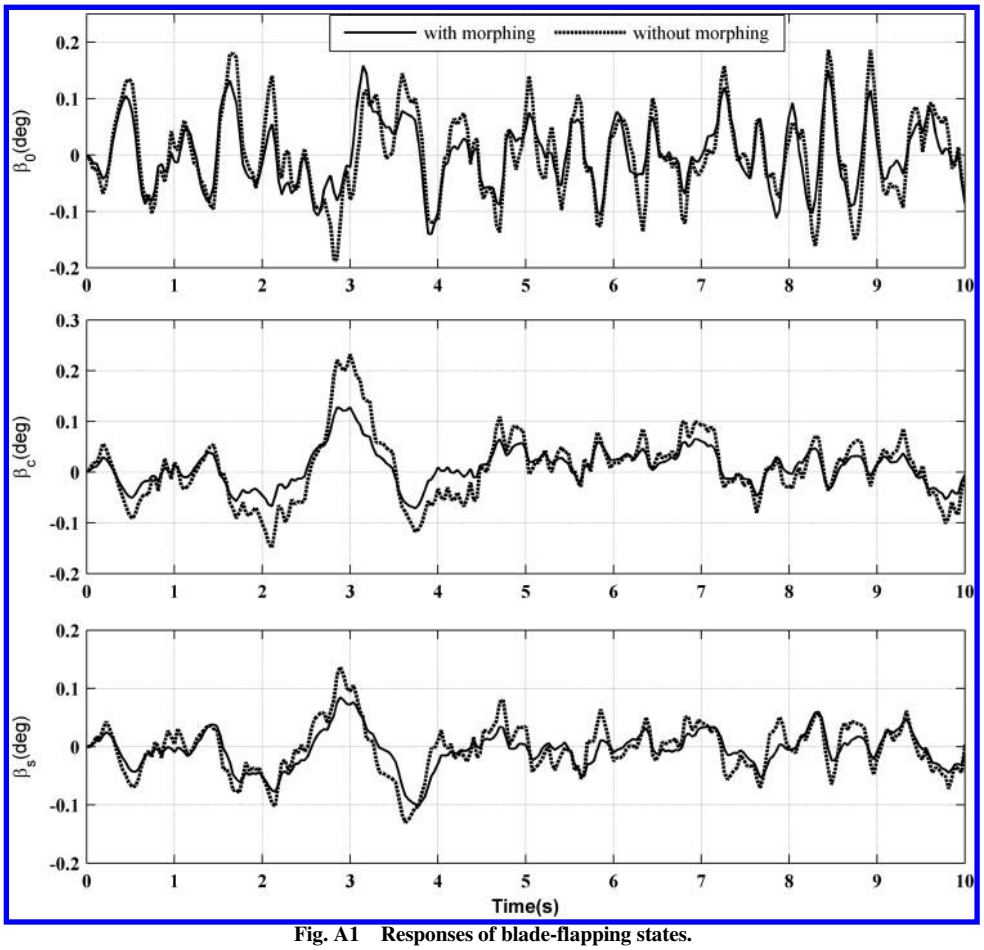

Fig. A1 Responses of blade-flapping states.

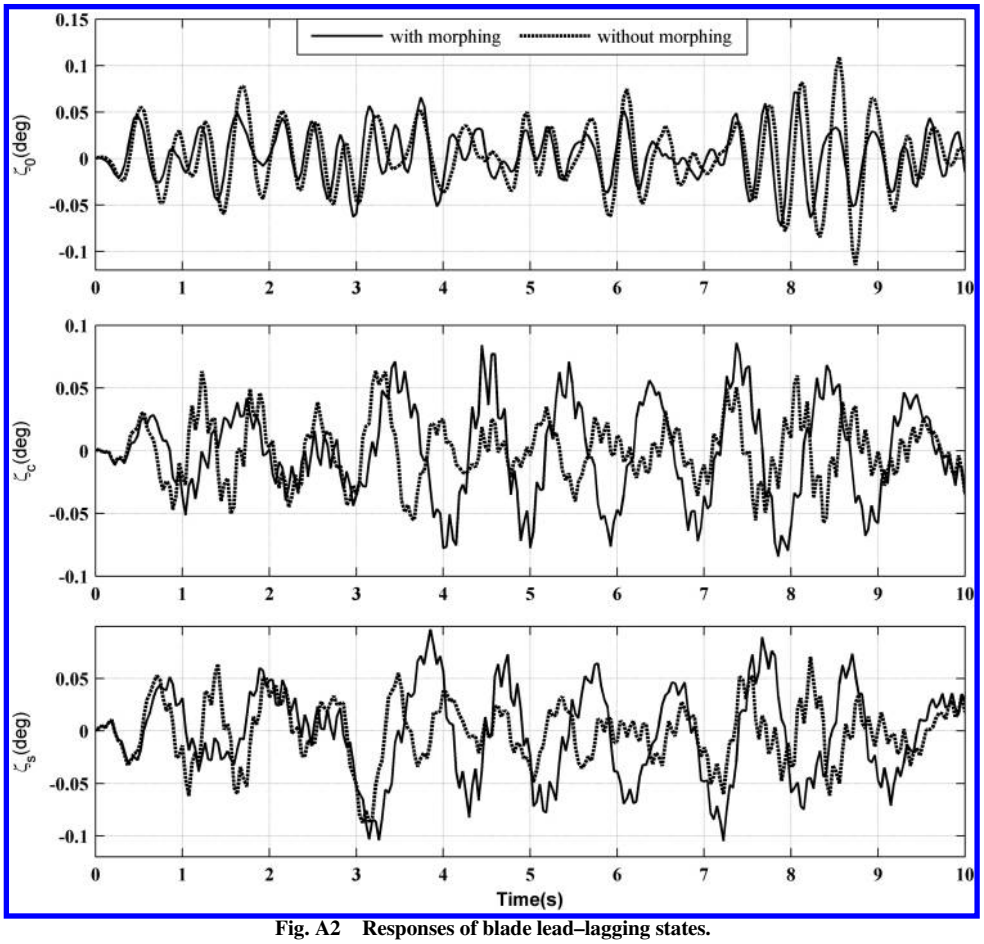

Fig. A2 Responses of blade lead–lagging states.

scenarios (i.e., with and without morphing). The observations made in the previous paragraph about flapping states are also valid for lead–lagging states. For instance, blade-lagging states do not experience dangerous behavior, and the qualitative and quantitative behaviors are similar for conventional (i.e., without morphing) and morphing helicopters.

In Figs. A3, A4, closed-loop responses of some blade-flapping angular velocity states (i.e., collective and two cyclic components) and blade-lagging states (i.e., collective and two cyclic components) are given for both scenarios, revealing the fact that the observations made for the previous two examples are valid for these states also.

Acknowledgment

The support of United Technologies Research Center for our helicopter work is gratefully acknowledged.

Downloaded by ROKETSAN MISSLES INC. on March 21, 2014 | http://arc.aiaa.org | DOI: 10.2514/1.C032494

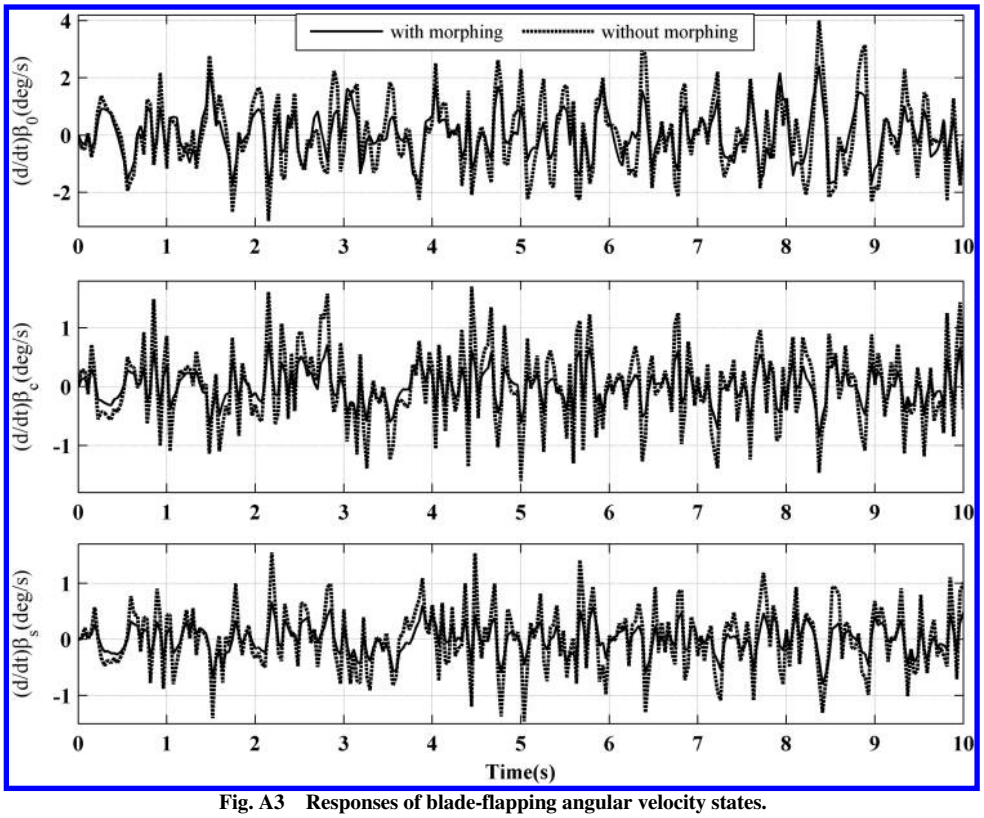

Fig. A3 Responses of blade-flapping angular velocity states.

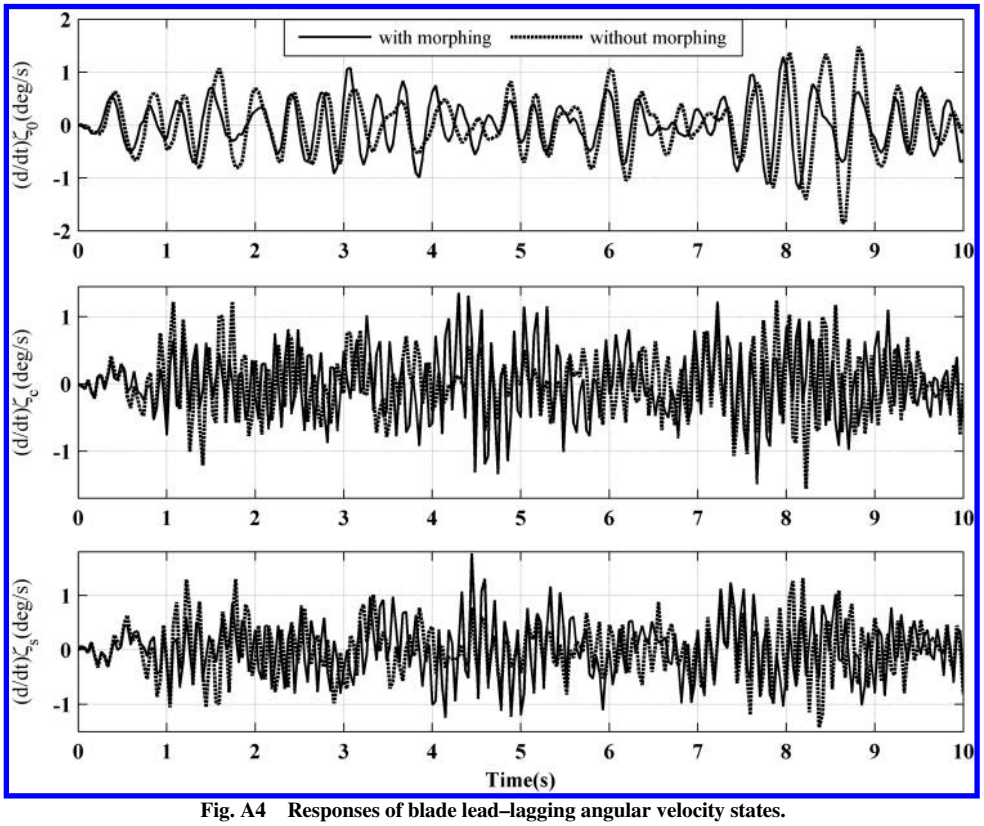

Fig. A4 Responses of blade lead–lagging angular velocity states.

References

[1] Iwata, T., and Rock, S. M., "Benefits of Variable Rotor Speed in Integrated Helicopter/Engine Control," *AIAA Guidance, Navigation, and Control Conference*, AIAA Paper 1993-3851, Aug. 1993.

[2] Guo, W., and Horn, J. F., "Rotor State Feedback Control for Rotorcraft with Variable Rotor Speed," *AIAA Guidance, Navigation, and Control Conference*, AIAA Paper 2009-5797, Aug. 2009.

[3] Horn, J. F., Guo, W., and Ozdemir, G. H., "Use of Rotor State Feedback to Improve Closed-Loop Stability and Handling Qualities," *Journal of the American Helicopter Society*, Vol. 7, No. 2, April 2012, pp. 1–10.

[4] Sekula, M., Wilbur, M., and Yeager, W., "Aerodynamic Design Study of an Advanced Active Twist Rotor," *Proceedings of the American Helicopter Society 4th Decennial Specialists' Conference on Aeromechanics*, American Helicopter Society, Alexandria, VA, 2004.

[5] Wilbur, M., and Sekula, M., "The Effect of Tip Geometry on Active Twist Rotor Response," *Proceedings of the American Helicopter Society Annual Forum*, American Helicopter Society, Alexandria, VA, 2005.

[6] Prabhakar, T., and Gandhi, F., "A Centrifugal Force Actuated Variable Span Morphing Helicopter Rotor," *Proceedings of the American Helicopter Society Annual From*, American Helicopter Society, Alexandria, VA, 2007.

[7] Yeo, H., "Assessment of Active Controls for Rotor Performance Enhancement," *Journal of the American Helicopter Society*, Vol. 53, No. 2, 2008, pp. 152–163. doi:10.4050/JAHS.53.152

[8] Kang, H., Saberi, H., and Gandhi, F., "Dynamic Blade Shape for Improved Helicopter Rotor Performance," *Journal of the American Helicopter Society*, Vol. 55, No. 3, 2010, pp. 1–11. doi:10.4050/JAHS.55.032008

[9] Khoshlahjeh, M., Barbarino, S., Gandhi, F., and Webster, S., "Helicopter Performance Improvement with Variable Chord Morphing Rotors," *Proceedings of the European Rotorcraft Forum*, Paris, 2010.

[10] Khoshlahjeh, M., Gandhi, F., and Webster, S., "Extendable Chord Rotors for Helicopter Envelope Expansion and Performance Improvement," *Proceedings of the American Helicopter Society Annual Forum*, American Helicopter Society, Alexandria, VA, 2011.

[11] Barbarino, S., Gandhi, F., and Webster, S., "Design of Extendable Chord Sections for Morphing Helicopter Rotor Blades," *Journal of Intelligent Material Systems and Structures*, Vol. 22, No. 9, Aug. 2011, pp. 891–905.

[12] Oktay, T., and Sultan, C., "Simultaneous Helicopter and Control System Design," *Journal of Aircraft*, Vol. 50, No. 3, 2013, pp. 911–926. doi:10.2514/1.C032043

[13] Oktay, T., and Sultan, C., "Constrained Predictive Control of Helicopters," *Journal of Aircraft Engineering and Aerospace Technology*, Vol. 85, No. 1, 2013, pp. 32–47. doi:10.1108/00022661311294021

[14] Oktay, T., "Constrained Control of Complex Helicopter Models," Ph.D. Dissertation, Virginia Polytechnic Inst. and State Univ., Blacksburg, VA, May 2012.

[15] Fusato, D., and Celi, R., "Multidisciplinary Design Optimization for Helicopter Aeromechanics and Handling Qualities," *Journal of Aircraft*, Vol. 43, No. 1, 2006, pp. 241–252. doi:10.2514/1.7943

[16] Fusato, D., Guglieri, G., and Celi, R., "Flight Dynamics of an Articulated Rotor Helicopter with an External Slung Load," *Journal of the American Helicopter Society*, Vol. 46, No. 1, 2001, pp. 3–14. doi:10.4050/JAHS.46.3

[17] Sahasrabudhe, V., Tischler, M., Cheng, R., Stumm, A., and Lavin, M., "Balancing CH-53K Handling Qualities and Stability Margin Requirements in the Presence of Heavy External Loads," *Proceedings of the American Helicopter Society 63rd Forum*, American Helicopter Society, Alexandria, VA, May 2007.

[18] Apkarian, P., Champetier, C., and Magni, J. F., "Design of a Helicopter Output Feedback Control Law Using Modal and Structured-Robustness Techniques," *International Journal of Control*, Vol. 50, No. 4, 1989, pp. 1195–1215. doi:10.1080/00207178908953426

[19] Altug, E., Ostrowski, J. P., and Mahony, R., "Control of a Quadrotor Helicopter Using Visual Feedback," *Proceedings of the IEEE International Conference on Robotics and Automation*, IEEE Publ., Piscataway, NJ, 2002, pp. 72–77.

[20] Ivler, C. M., Tischler, M. B., and Powell, J. D., "Cable Angle Feedback Control Systems to Improve Handling Qualities for Helicopters with Slung Loads," *AIAA Guidance, Navigation, and Control Conference*, AIAA Paper 2011-6686, Aug. 2011.

[21] Huang, C. Y., Celi, R., and Shih, I. C., "Reconfigurable Flight Control Systems for a Tandem Rotor Helicopter," *Journal of the American Helicopter Society*, Vol. 44, No. 1, 1999, pp. 50–62. doi:10.4050/JAHS.44.50

[22] Jiang, Z., Han, J., Wang, Y., and Song, Q., "Enhanced LQR Control for Unmanned Helicopter in Hover," *Proceedings of the 1st International Symposium on Systems and Control in Aerospace and Astronautics*, Harbin, China, 2006, pp. 1438–1443.

[23] Zhang, Z. W. M. D., and Wu, J., "Hovering Control and Simulation of a Tandem Helicopter Using LQR Approach," *Microcomputer Information*, Vol. 25, 2010, p. 73.

[24] Bo, L. Y., Zhu, L. W., and Qi, S., "Improved LQG Control for Small Unmanned Helicopter Based on Active Model in Uncertain Environment," *Proceedings of the International Conference on Electronics, Communications and Control (ICECC)*, Ningbo, China, 2011, pp. 289–292.

[25] Luo, C. C., Liu, R. F., and Chang, Y. H., "Helicopter H_∞ Control Design with Robust Flying Quality," *Aerospace Science and Technology*, Vol. 7, No. 2, 2003, pp. 159–169. doi:10.1016/S1270-9638(02)00012-3

[26] Kureemun, R., Walker, D. J., Manimala, B., and Voskuijl, M., "Helicopter Flight Control Law Design Using H_∞ Techniques," *Proceedings of the IEEE Conference on Decision and Control and the European Control Conference*, IEEE Publ., Piscataway, NJ, 2005, pp. 1307–1312.

[27] Xie, R., Wang, X., and Li, Y., "H_∞ State Feedback Control for the Stabilization of the Three Euler Angles of Helicopter Based on LMI," *Proceedings of the International Conference on Intelligent Computation Technology and Automation*, Hunan, China, 2008, pp. 375–379.

[28] Oktay, T., and Sultan, C., "Variance Constrained Control of Maneuvering Helicopters with Sensor Failure," *Journal of Aerospace Engineering*, Vol. 227, No. 12, 2013, pp. 1845–1858. doi:10.1177/0954410012464002

[29] Spall, J. C., "Multivariable Stochastic Approximation Using a Simultaneous Perturbation Gradient Approximation," *IEEE Transactions on Automatic Control*, Vol. 37, No. 3, 1992, pp. 332–341. doi:10.1109/9.119632

[30] Sultan, C., "Proportional Damping Approximation Using the Energy Gain and Simultaneous Perturbation Stochastic Approximation," *Mechanical Systems and Signal Processing*, Vol. 24, No. 7, 2010, pp. 2210–2224. doi:10.1016/j.ymssp.2010.02.013

[31] Leishman, J. G., *Principles of Helicopter Aerodynamics*, Cambridge Univ. Press, Cambridge, England, U.K., 2006, p. 160.

[32] Padfield, G. D., *Helicopter Flight Dynamics*, AIAA Education Series, AIAA, Reston, VA, 2007.

[33] Skelton, R. E., *Dynamic Systems Control: Linear Systems Analysis and Synthesis*, Wiley, New York, 1987, Chap. 8.

[34] Skelton, R. E., Iwasaki, T., and Grigoriadis, K., *A Unified Algebraic Approach to Linear Control Design*, Taylor and Francis, Washington, D.C., 1998, Chap. 4.

[35] Skelton, R. E., and Lorenzo, M. D., "Space Structure Control Design by Variance Assignment," *Journal of Guidance, Control, and Dynamics*, Vol. 8, No. 4, 1985, pp. 454–462. doi:10.2514/3.20005

[36] Hsieh, C., Skelton, R. E., and Damra, F. M., "Minimum Energy Controllers with Inequality Constraints on Output Variances," *Optimal Control Application and Methods*, Vol. 10, No. 4, 1989, pp. 347–366. doi:10.1002/oca.4660100405

[37] Zhu, G., and Skelton, R. E., "Mixed L_2 and L_∞ Problems by Weight Selection in Quadratic Optimal Control," *International Journal of Control*, Vol. 63, No. 5, 1991, pp. 1161–1176.

[38] Zhu, G., Rotea, M. A., and Skelton, R. E., "A Convergent Algorithm for the Output Covariance Constraint Control Problem," *SIAM Journal on Control and Optimization*, Vol. 35, No. 1, 1997, pp. 341–361. doi:10.1137/S0363012994263974

[39] Sultan, C., "Decoupling Approximation Design Using the Peak to Peak Gain," *Mechanical Systems and Signal Processing*, Vol. 36, No. 2, 2013, pp. 582–603. doi:10.1016/j.ymssp.2012.10.007

[40] He, Y., Fu, M. C., and Marcus, S. I., "Convergence of Simultaneous Perturbation Stochastic Approximation for Non-Differentiable Optimization," *IEEE Transactions on Aerospace and Electronic Systems*, Vol. 48, No. 8, 2003, pp. 1459–1463.

Downloaded by ROKETSAN MISSLES INC. on March 21, 2014 | http://arc.aiaa.org | DOI: 10.2514/1.C032494

[41] Sadegh, P., and Spall, J. C., "Optimal Random Perturbations for Multivariable Stochastic Approximation Using a Simultaneous Perturbation Gradient Approximation," *IEEE Transactions on Automatic Control*, Vol. 43, No. 10, 1998, pp. 1480–1484. doi:10.1109/9.720513

[42] Oktay, T., and Sultan, C., "Modeling and Control of a Helicopter Slung-Load System," *Aerospace Science and Technology*, Vol. 29, No. 1, 2013, pp. 206–222. doi:10.1016/j.ast.2013.03.005

[43] Oktay, T., and Sultan, C., "Variance Constrained Control of Maneuvering Helicopters," *Proceedings of the American Helicopter Society 68th Annual Forum*, American Helicopter Society, Alexandria, VA, May 2012.

[44] Oktay, T., and Sultan, C., "Integrated Maneuvering Helicopter Model and Controller Design," *AIAA Guidance, Navigation and Control Conference*, AIAA Paper 2012-4596, Aug. 2012.

[45] Oktay, T., and Sultan, C., "Robustness of Variance Constrained Controllers for Complex Helicopter Models," *Proceedings of the American Control Conference*, Washington, D.C., June 2013, pp. 794–799.

Downloaded by ROKETSAN MISSLES INC. on March 21, 2014 | http://arc.aiaa.org | DOI: 10.2514/1.C032494